Applied Energy 378 (2025) 124718

Contents lists available at ScienceDirect

Applied Energy

journal homepage: www.elsevier.com/locate/apenergy

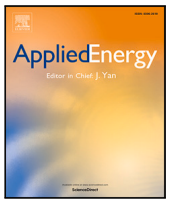

Optimizing energy storage capacity for enhanced resilience: The case of offshore wind farms

Weijie Pan *, Ekundayo Shittu

Department of Engineering Management and Systems Engineering, The George Washington University, Washington, DC, 20052, USA

ARTICLE INFO

Keywords:
Battery energy storage system
Clustering method
Network topology
Offshore wind farm
System resilience

ABSTRACT

This paper investigates the influence of different configurations of the offshore wind farms (OWF) network on the optimal capacities of battery energy storage systems (BESS) in the face of high-impact low-probability (HILP) events that cause short- to medium-term outages. Large-scale OWFs have garnered increasing attention from investors due to their smaller land footprint and higher energy production potential. However, the external environment, the internal installation, and the long distance from the onshore facilities pose significant challenges to the operations of the OWFs and the stability of the energy supply. These factors render systems highly susceptible to HILP contingencies, while timely post-disaster management, such as addressing subsea transmission cable failures, is challenging. Although BESS has long been considered a viable strategy to improve the resilience of the system, the decision-making process to determine the optimal BESS capacity is underexplored. This is more pronounced when considering the diverse OWF topologies that can significantly impact energy supply efficiency and, consequently, impact the stable operation of BESS. This study employs a methodology based on sequential "planning + operational" modeling approach that integrates Agglomerative Hierarchical Clustering (AHC), an optimal OWF network configuration algorithm, a stochastic system failure scenario generation approach, and an optimal BESS capacity model. Comprehensive profiles of optimal BESS capacity are derived corresponding to different clustering levels. Applying the proposed model to three different OWF cases derived the optimal BESS capacity, balancing resilience enhancement and economic considerations. In the context of the modeling settings in this study, this optimal capacity is approximately 16% of the daily electricity generation at full capacity, excluding the capacity factor. Optimal BESS capacity not only standardizes and facilitates the design process of more resilient OWFs to short- and medium-term system failures, but also provides policymakers with a basis to consider and implement strategies to coordinate the use of OWF energy and other available power generation technologies in the market. This study bridges the research gap between OWF topology studies and discussions on system resilience while shedding light on the relationship between optimal BESS capacities and the ideal number of clusters.

1. Introduction

The primary objective of this study is to investigate the optimal capacity of the battery energy storage system (BESS) within independent offshore wind farms (OWF) with the aim of bolstering their resilience. There is no doubt that clean energy policies continue to yield the dividends of decarbonizing the power sector through the increasing proportion of electricity generated from renewable sources, such as wind turbines (WT) and photovoltaic systems [1–4]. However, the inherent intermittency of renewable energy resources, coupled with the escalating occurrence of extreme weather events and malicious human attacks, presents a challenge on how to ensure the stability of energy systems and fortify their resilience [5–7]. One of the well-investigated approaches is the use of storage technologies. Despite their growing prominence and adoption, there are still challenges related to determining their optimal sizes and capacities [8,9]. Specifically, oversized storage could imply under-utilization of funds for excess capacities, while under-sized storage could portend inadequacies. Both situations could have negative impacts on both operations and resource utilization.

This study is motivated by the global trend of increasing wind energy development, where large-scale wind farms located in remote areas such as mountains, deserts, and coastal regions are drawing increasing interest from investors [10,11]. Among these developments,

* Correspondence to: Department of Engineering Management and Systems Engineering, The George Washington University, 800 22nd Street NW, Washington, DC, 20052, USA.
E-mail addresses: weijiepan93@gwu.edu (W. Pan), eshittu@gwu.edu (E. Shittu).

https://doi.org/10.1016/j.apenergy.2024.124718
Received 29 May 2024; Received in revised form 16 August 2024; Accepted 14 October 2024

Acronyms list	
Acronyms	Description
AHC	Agglomerative hierarchical clustering
BESS	Battery energy storage systems
HILP	High-impact,Low-probability
HPLI	High-probability,Low-impact
LCOE	Levelized cost of electricity
OCP	Onshore substation/Onshore common point
OWF	Offshore wind farms
SUB	Offshore substation
WT	Wind turbine

OWFs receive considerable attention due to their lower land footprint and higher energy production potential driven by stronger offshore winds, which leads to a more extensive deployment of large-scale OWFs [11–13]. For example, the capacity of US offshore wind energy projects under development and currently operational in 2023 has increased by 15% compared to 2022, reaching more than 52 GW. If fully developed, these projects could provide enough energy to power more than 18 million American homes [14]. However, OWFs face threats both from the external environment and from internal technical flaws [15]. Among all system faults, WTs failures and subsea transmission cables faults are the primary issues that significantly impact system operations. Although the failure rate for WTs is higher than that for subsea transmission cables — 9.06 failures per turbine per year [16] compared to 0.003 failures per kilometer per year [17] — the consequences of transmission cable failures are more severe. In general, 80% of all financial losses and insurance claims are attributed to power cable failures [18,19]. Depending on the specific failure situation, the associated repair time for transmission cable failures can range from a few hours to several months [18,20]. In some severe cases, repairing interarray cables takes about 40 days and incurs approximately $2 million in damage costs. For export cables, repairs take around 60 days, with damage costs ranging from $10 million to $30 million. In any circumstance, the long distance from the onshore facilities makes the post-disaster restoration process for OWFs more challenging and costly than for the onshore technologies [21]. Therefore, it is imperative to improve the resilience of OWFs and mitigate the threats posed by high-impact, low-probability (HILP) events [22].

It should be mentioned that the concept of resilience has been widely accepted as an indicator to assess dynamic restoration performance after normal operation of a system has been disrupted by HILP events [23]. Unlike statistical indices such as reliability that measure a system's ability to hedge against high-probability but low-impact (HPLI) contingencies, resilience evaluation typically includes four stages: prevention, degradation, restoration, and adaptation [24]. Applying this framework to OWFs, a notable challenge arises in the form of the need for long-distance transmission cables to link all WTs and connect them to the onshore power grid [25,26]. As mentioned above, a fault cable can stop the transmission of electricity generated from a group of WTs, exemplifying a HILP event for OWFs [10]. Interestingly, the layout of the transmission cables in the OWF is closely related to its design topology [27], which ultimately affects the efficiency of energy production. Therefore, it is imperative to explore the relationship between resilience-oriented system planning and OWF topology.

Numerous strategies have been investigated to enhance the resilience of power systems [7,28–30], encompassing optimal power distribution from multiple energy sources, the establishment of networked microgrids with adaptable structural configurations, and the active participation of electricity consumers. However, when it comes to OWFs, which are often far from energy consumers and operate in a relatively isolated manner, traditional methods for improving resilience may not be applicable. BESS stands out as one of the most popular solutions for addressing the intermittency of renewable energy sources, predictive errors, and participation in the electricity market [1]. BESS not only contributes to the improvement in power system reliability, but also shows compatibility with a variety of energy technologies [31,32]. Technically, the interoperability of OWFs and BESS has been studied and verified as a feasible solution to provide black start capability to power grids [33,34]. Economically, a battery integrated with a wind farm can create greater value than a standalone battery [35]. This is supported by the conclusion of another study that OWFs with a larger number of WTs are more resilient when economic capacity is sufficient [36]. Hence, considering the practical feasibility of BESS in terms of service duration, BESS emerges as a robust option to improve resilience against short- to medium-term system failures, which can result in degraded system operation lasting from a few hours to a few days at most.

To our knowledge, there is a gap in the existing literature on the assessment of BESS capacities with a resilience-oriented approach in various OWF layout structures and the exploration of their relationships. Concisely, the central research question posed in this study is as follows: How do OWF topologies influence the determination of the optimal BESS capacity? This study employs a sequential modeling approach that encompasses both the planning and operational phases. During the planning phase, the optimal network configuration for OWFs is determined, while in the operational phase, the optimal BESS capacity is determined. The operational phase also integrates HILP event scenarios, simulating system faults that disrupt the normal operations of OWFs. The optimal BESS capacity is expected to vary depending on various OWF topologies. However, through the systematic construction of various OWF topologies, a comprehensive profile of the optimal BESS capacity can be obtained, allowing the identification of an appropriate BESS capacity for the system as a whole. This ultimate BESS capacity is designed to compensate for energy shortfalls resulting from HILP events, and it can adapt to any scenario where the collection system needs reconfiguration to mitigate the cascading effects of a system fault. A detailed methodology describing these processes is presented in Section 3.

The proposed methodology has been applied to three OWFs with varying layouts and installed capacities. The modeling results reveal several key findings: (1) the OWF topologies do, in fact, influence the decision on the optimal BESS capacity; (2) as the number of WT clusters increases, the profile of the optimal BESS capacity tends to converge, indicating that there are diminishing returns to the cluster sizes in terms of storage; and (3) the optimal BESS capacity, in the context of the modeling settings in this study, is approximately 16% of the daily electricity generation at full capacity of the entire OWF, without considering the capacity factor.

This study makes three significant contributions. First, the proposed methodology bridges the research gap that has traditionally separated studies on OWF configurations from those focused on OWF resilience. Second, it shifts the perspective on BESS capacity from a deterministic variable tailored to a specific system structure to a more versatile and generalized approach applicable to a wide range of OWF topologies.

Third, it elucidates the relationship between the optimal BESS capacity and the optimal WT cluster number, revealing that these two elements need not be synchronized and can be independently selected in practical applications.

2. Literature review

Previous research on OWFs can be broadly categorized into two main streams: planning phase studies and operational phase studies. Planning phase studies primarily focus on configuring the collector systems, while operational phase studies tend to assess system performance under uncertain conditions. Furthermore, there is also room for joint consideration of both phases in the context of reliability assessment studies. Some studies have highlighted the importance of strengthening resilience when integrating OWFs into conventional power grids. These works have undeniably provided valuable insight into OWFs from both theoretical and practical standpoints. However, a noticeable research gap persists, characterized by a disconnect between resilience-oriented investigations and comprehensive "planning + operation" studies in OWFs.

First, in OWF planning phase studies, the primary focus lies in optimizing the system topology. These studies aim to minimize investment costs and often involve the comparison of different computational algorithms as their main research objectives. Research in this domain, which focuses on optimizing the layout of wind farms and the configuration of the collector system, has been extensively reviewed in previous works [37–39]. In summary, the general objective of optimizing the layout of an OWF usually revolves around minimizing the total length of transmission cables [40] and/or reducing the overall economic cost of establishing the entire network of the system [41]. Within this body of work, the clustering of WTs has emerged as an effective strategy to ease computational burdens and improve the reliability of the energy supply [42]. Furthermore, the design and placement of multiple offshore substations are gaining traction among researchers, as they help streamline the solution search space for network configurations [43]. These configuration studies, to some extent, align more closely with principles from graph theory and operations research, somewhat distancing themselves from the intricate characteristics of energy systems.

Second, in recognition of the significant uncertainties that arise from unpredictable environmental factors that influence power generation, such as wind speed, typhoon trajectories, and wake effects, certain studies focus on developing predictive models to accurately capture these environmental characteristics [44,45]. Their objective is to improve energy supply stability by modifying existing OWF structures or designing optimal OWF topologies, all while considering those uncertainties. However, it is essential to note that the results of these studies may be constrained by the low resolution of available data samples or limited in generalizability due to unique geological conditions [39]. Nevertheless, it is noteworthy that, from a macro-perspective, the energy production from OWFs exhibits relative smoothness over time, particularly when compared to solar energy, which follows a parabolic pattern with periods of zero solar insulation during the evening hours. In this broader context, despite the presence of environmental uncertainties, power generation can still be regarded as a continuous output, provided that the research objective does not require absolute numerical accuracy.

Third, studies focusing on the reliability of OWFs can be viewed as a harmonious blend of both the planning and operational phases, with environmental uncertainties serving as significant external drivers affecting system performance. For example, methodologies described in works like [46,47] share a common approach to designing the economic outer and inner layers of OWFs. Their objective is to minimize the sum of construction costs, power losses, maintenance expenses, and reliability costs, all while accounting for cable outages initiated by uncertain external impacts. In addition, the reliability assessment also includes considerations of topology. For example, in [48], the feasibility of achieving a balance between economical planning and reliable operation through the interconnection of WTs in a multi-loop configuration with cables of small cross-sectional areas has been confirmed. They also explore the possibility of reducing transformer capacity and sharing it through cross-substations. In another study [49], the failure rate of the components of the collector system and their corresponding repair rates are integrated into the reliability evaluation process. Here, primary evaluation indices include power generation rates and expected energy not supplied. These insights derived from reliability studies offer robust support for further research oriented towards enhancing resilience, particularly when accounting for post-disaster scenarios.

Studies on OWF resilience have gained significant traction, encompassing a wide spectrum of aspects. These investigations span from the technical design of robust WT components [50] to bolstering resilience in power systems through the integration of OWFs into onshore power grids. They even extend to post-disaster maintenance and recovery support management for OWFs [21], slightly veering into aspects beyond the purely technical domain. Although component design and human-based support management studies lie outside the scope of the current research objective, it is valuable to review the remaining resilience-oriented studies that focus on OWF operations, particularly restoration strategies. With the rapid advancement of grid-connection technology, OWFs are increasingly integrated into provincial power grids to enhance generation capacity and improve penetration of clean energy. For example, studies such as [51] demonstrate that accepting the limited risks associated with participation of OWFs in the power grid restoration process can significantly reduce restoration time and minimize user losses. Furthermore, the resilience of the power system during extreme typhoon events can be strengthened through coordinated on/off states and active power output of conventional onshore units, multiple offshore OWFs, and energy storage stations. This coordination is based on a robust distributional chance constraint-based model proposed in [52]. However, it is important to note that these resilience-oriented studies often treat OWFs as vital components or subsystems within a larger power grid context, as exemplified in [53]. In such cases, decision-making models are designed to improve the robustness of optimal power flow in the presence of OWFs. Those studies do not position OWFs as independent systems. In other words, while the overall resilience performance or the coordination of subsystems within an integrated system is addressed, the intrinsic resilient operational performance of OWFs themselves is not the primary focus.

In the context where OWFs are considered independent energy supply systems, the importance of BESS becomes evident in bolstering system resilience by ensuring a continuous energy supply to consumers during power outage scenarios. For example, in [1], the characteristics of fluctuation of the power play a central role in determining the optimal storage capacity within a hybrid wind-battery energy system. Similar investigations of the BESS capacity for wind power have been conducted using stochastic models in [54,55]. However, these optimal solutions tend to be deterministic and lack generalizability, as they are tailored to specific systems, akin to the earlier discussion on optimal topology design under uncertainties. Recognizing this limitation, a standardized multi-objective decision making framework is introduced in [13]. This framework allows OWF planners to select the most suitable BESS from a given range of capacities. Its primary objective is to minimize the discrepancy between forecasted and actual power output, a discrepancy influenced by uncertain wind speeds and wake effects. In particular, in this study, the BESS capacity is treated as a predetermined parameter, rather than a stochastic decision variable, limiting its flexibility and adaptability in system design. As also underscored in [13], while many studies have emphasized the economic and operational aspects of BESS, not enough attention has been paid to reliability issues when determining the capacity of BESS.

Table 1
Taxonomy of methodologies for selected OWF studies and their key conclusions. (Note × shows absence).

References	Model objective(s)	Optimal configuration	Placement of SUB/WTs	Operational uncertainty	Backup capacity	Key research conclusion(s)
[1]	*min*(System cost), *min*(Power mismatch)	×	×	Wind speed, wake effect	Unknown capacity	The optimal battery capacity can be determined on the basis of long-term wind speed data and WT layout.
[13]	*min*(Power output mismatch)	×	×	Wind speed, wake effect, WT failures	Given capacity	A long-duration BESS is better for avoiding energy issues and power cuts, but a medium-duration BESS gives a higher financial return.
[51]	Load restoration	×	×	WT failures to typhoon and lightning stroke	×	Adding OWFs to power grids can shorten restoration time and provide financial benefits, with system inertia and repair costs being important factors.
[49]	Reliability evaluation on power generation	×	×	Unpredictable wind speed	×	Seasonal wind speed and collection system component failures are key factors in assessing the reliability of OWFs.
[53]	*min*(Power purchase cost)	×	×	Installed capacities of OWFs, OWF location uncertainty	×	OWF location impacts costs; higher generation sensitivity lowers uncertainty tolerance, while higher procurement costs allow greater uncertainty.
[26]	Reliability evaluation on configuration design	×	×	Components failure	×	Having alternative transmission paths enhance reliability during faults, but a meshed DC grid is costly. Bipole transmission offers a more cost-effective solution for mitigating HILP failures.
[52]	Optimal power dispatch	×	×	Uncertain typhoon parameters	×	Jointly optimizing the on/off states and power outputs of conventional units, WTs, and energy storage stations can enhance resilience during extreme typhoon events.
[41]	*min*(LCOE of non-homogeneous OWF)	Genetic algorithm	×	×	×	Even with higher energy output, non-homogeneous turbine layouts may not be cost-effective for developers in terms of LCOE.
[40]	*min*(Capital cost), Capacitated MSP	Shortest path	*Kmeans*++ clustering	×	×	The sequential design approach for inter-array cables in OWFs efficiently automates and optimizes the layout by dividing it into smaller problems.
[43]	*min*(Investment cost)	Prim's algorithm	Genetic algorithm	×	×	Encoding OWF topology into a binary string efficiently considers optimal connections and reduces infeasible configurations, thereby streamlining the search for solutions.
[56]	*min*(Investment cost), *max*(Energy output)	×	Particle swarm algorithm (PSO)	Wind speed and direction	×	The developed wake model effectively calculates wake losses and optimizes regular-shaped wind farm layouts using the PSO algorithm.
[42]	Optimize configuration, Enhance reliability	Meshed connection	PSO, Hierarchical clustering	Fixed outage rate	×	A novel two-level approach using the average linkage AHC algorithm effectively determines optimal cabling and connection topologies for HVDC-connected offshore wind farms.
This study	*min*(Investment and operational cost)	Minimal spanning tree method	Hierarchical clustering	Stochastic power curtailment scenarios	Unknown capacity	OWF configurations significantly impact the decision-making process to determine the optimal capacity of BESS to improve system resilience.

A taxonomy of methodologies for the selected OWF studies and their key conclusions is presented and compared in Table 1. The link between studies that emphasize OWF configurations and those that focus on OWF reliability and resilience remains somewhat obscure. There is potential value in simultaneously exploring the OWF topology and improving resilience. In light of this research gap, this study aims to investigate the fundamental connections between the optimal capacity of the BESS and the OWF configuration structures.

3. Methodology

In summary, in this study, OWFs are treated as independent systems, with onshore BESS serving as the only technology capable of ensuring the stability of the energy supply when normal operations are compromised. BESS is assumed to be located at an onshore substation. This assumption is supported by a previous study, which concluded that the battery system generated higher revenues when located onshore [57]. As mentioned earlier, considering the varying repair times required for different maintenance categories, as summarized in Table 2, and the practical operational duration of BESS, this study focuses only on short- to medium-term degraded system failures, which typically last from hours to a few days at most. Long-term system failures, which last from weeks to months, are impractical for BESS to effectively address to maintain the energy supply over such extended periods and are thus beyond the scope of this study.

Table 2
Taxonomy of OWF maintenance categories and associated repair times. (Note ✓indicates a match).

Maintenance categories	Estimated repair time	Short/Medium-term	Long-term
Repair for WT	2~20 h [20,58]	✓	
Replacement of WT components	8~40 h [20,58]	✓	
Repair in transformer station	4~60 h [20]	✓	
Repair to foundation/scour protection	4~12 h [20]	✓	
Cable replacement	20 h~60 days [18,20]	✓	✓

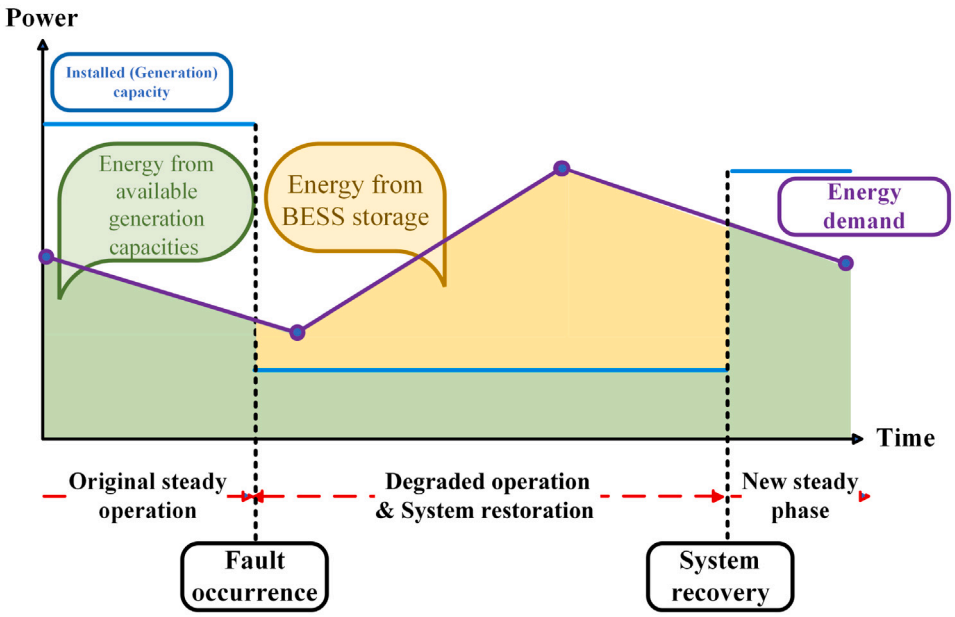

Fig. 1. Illustrative resilience concept.

The resilience concept in this study is visually depicted in Fig. 1.

In this scenario, the backup energy from BESS is utilized to compensate for the energy not supplied due to the disconnection of the entire impacted cluster of WTs resulting from a main transmission cable fault. During the phase of degraded system operation, a post-disaster management team plays a crucial role in restoring the system. Once the system's normalcy is restored, BESS discharging is deactivated, and recharging continues until full capacity is reached. In theory, the maximum BESS capacity can be identified in the worst-case scenario, where the entire OWF is disconnected from the onshore substation. However, conducting a comprehensive assessment that incorporates economic considerations and time-dimensional uncertainties with respect to HILP events complicates the decision-making process to determine the optimal capacity of BESS. Likewise, while this worst-case scenario might offer the requisite BESS capacity, it should be noted that the likelihood of such catastrophic system-wide collapse only exists at the tail of the distribution of failures to OWFs. As such, making decisions on that total capacity may be exorbitant or cost-inefficient. However, inadequate BESS capacity may also not meet the desired expectation of achieving resilience in the aftermath of a failure. Hence, the optimal sizing of the BESS is based on the expected capacity required to address likely system failure scenarios.

To explore the impact of optimal OWF topology on the decision-making process for optimal backup BESS capacity planning, with the goal of improving the resilience of the system, this study employs a sequential modeling approach. By integrating the likelihood of HILP contingencies occurring throughout the decision-making process, the proposed methodology simultaneously addresses both the system planning phase and the operational phase. The primary objective is to reinforce the validity of final decisions conditioned on both economic consideration and technical implication. The entire methodology framework, including the modeling flowchart, objectives, methods, assumptions, rationales, and available data sources, is illustrated in Fig. 2.

In implementing this sequential modeling methodology, certain assumptions need to be stated at each step, either to simplify the modeling process, reduce computational burden, or eliminate factors irrelevant to the research objectives. These assumptions, along with their rationales or justifications, are presented in Fig. 2. Among them, two main assumptions must be emphasized. First, uncertainties from external environmental factors, such as wind speed and wake effect, are ignored to simplify the modeling complexity and reduce computational burden. Instead, these uncertainties, which impact the output of the system generation, are captured as a measurement called the capacity factor [9], with a numerical value between 0 and 1. This assumption leads to a constant generation output profile from OWFs, as illustrated in Fig. 3. Second, the decision on the topology of the OWFs is based solely on their geographic locations, regardless of the aforementioned resource uncertainties. A fixed topology is established as a necessary step in modeling system operations. In this study, optimizing the topology of the system for resilience enhancement is not a focus but could be a potential direction for future research.

In the planning phase, all WTs within a given OWF are clustered using the Agglomerative Hierarchical Clustering (AHC) method [59]. This clustering process is crucial in this study because: (1) it forms the basis for subsequent optimal topology planning at a fixed clustering level, (2) it facilitates the examination of how topology variations

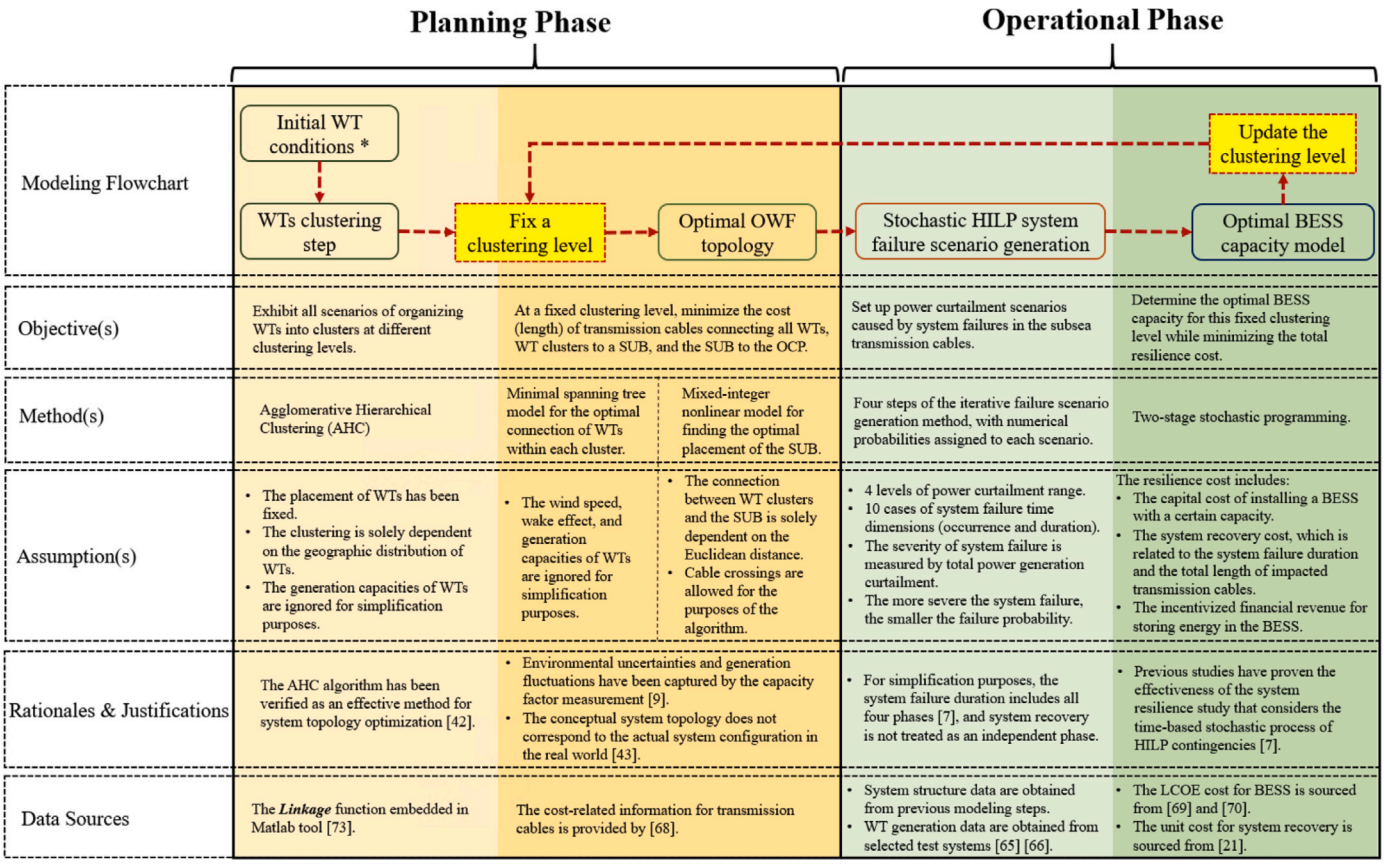

Fig. 2. Methodology framework and modeling step summaries.

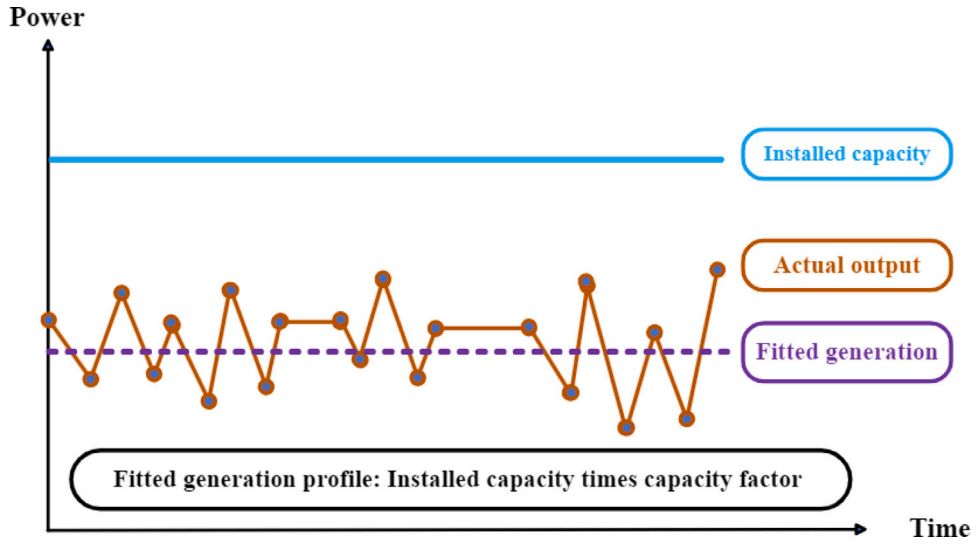

Fig. 3. Illustrative generation profile with capacity factor.

affect decisions regarding BESS capacity, and more importantly, (3) it prepares for modeling subsequent power curtailment scenarios by assuming transmission cable faults and isolating the fault zone during the operational phase. The AHC method dendrogram tree displays all possible combinations of WT clusters at each level of clustering. At a specified clustering level, optimal OWF topology planning involves configuring the connections among all WTs within each cluster and determining the placement for the offshore substation (SUB) that aggregates all clusters and connects to the onshore common point (onshore substation, OCP). The detailed AHC process and the methodology for achieving optimal OWF topology are presented in Sections 3.1 and 3.2, respectively.

Once the entire OWF topology is determined, HILP contingencies are introduced to influence system operations, with the aim of determining an optimal BESS capacity. The impacts of HILP events are generated using a scenario-based method that incorporates various power curtailment levels and all combinations of time dimensions for HILP events. The optimization model for determining the optimal BESS capacity is formulated as a two-stage mixed-integer linear programming problem, with the BESS capacity serving as the first-stage decision variable, and system operations, such as actual power generation amounts and the state of the battery system, being the second-stage decision variables. The scenario generation method is detailed in Section 3.3, and the optimization model for the optimal capacity of BESS is clarified in Section 3.4.

To justify the selection of two-stage stochastic programming in modeling the operational phase, the authors of this study acknowledge the existence of other modeling approaches. However, different approaches are intended to solve various problems and achieve different research objectives in the field of OWF studies. For example, with sufficient historical data, uncertainties such as wind speed can be modeled using Monte Carlo techniques and probabilistic analytical methods, as demonstrated in previous work [1,13,26,49]. In contrast, when data availability is limited, a discrete scenario-based approach can be used to capture uncertainties [60]. In such cases, two-stage stochastic programming is an effective tool to solve problems when the sample size of scenarios is under good control, as shown in previous research related to resilience enhancement [7,51,61].

The entire "planning + operational" modeling process will be implemented iteratively by selecting different clustering topologies from the AHC procedure, and will be terminated after exhausting all cluster topologies. This methodology allows for the derivation of a comprehensive profile of BESS capacities across different OWF topologies, with the aim of addressing the proposed research question.

3.1. Agglomerative hierarchical clustering (AHC)

The AHC method has been proven to be effective in previous studies in determining the optimal cabling and suitable topologies for OWFs [42]. The implementation of WT clustering within an OWF, based on AHC, is based solely on the geographic distribution of WTs, regardless of their energy generation capacities. The flexibility of AHC enables visualization of all possible clustering scenarios, making it a valuable preliminary step in the methodology of this study. A complete illustration of the AHC process is provided in Fig. 4.

The entire OWF is positioned within a Cartesian coordinate system, where each WT is assigned specific X and Y coordinates. The AHC algorithm automatically calculates the Euclidean distance between WTs and establishes the distance range for each possible cluster at varying levels of n clusters.

To illustrate, consider a small OWF with nine WTs, as depicted in Fig. 4. In the output of the AHC process, at the first level ($n = 1$), all WTs are treated as elements within a single cluster. At the third level ($n = 3$), WT_8, WT_9, WT_3, WT_5, and WT_6 form a cluster, while WT_1 and WT_2 constitute another cluster, and WT_4 and WT_7 form the final cluster.

Technically, the AHC process can continue until each individual WT is treated as a separate and independent cluster. However, in the context of this investigation, this scenario is considered invalid and is excluded. In other words, in this study, the smallest cluster needs to contain at least two WTs. In the illustration, the smallest valid cluster number is four, *i.e.*, $n = 4$. For generalization purposes, in an OWF with P WTs, the maximum number of clusters is defined as $\lfloor \frac{P}{2} \rfloor$.

3.2. Optimal OWF topology

The optimal OWF topology comprises two main aspects: the optimal configuration of WTs network and the optimal planning of WT clusters (the optimal placement of SUB). Regarding the former, the objective is to establish connections among all WTs within each cluster while minimizing the total length (and total cost) of the transmission cables. This aspect is addressed using the classical minimum spanning tree algorithm [62,63], which has been used in prior studies on OWFs and is appropriate given that it is assumed that all WTs experience uniform environmental conditions in the open ocean [40]. This differs from onshore wind farms, where WTs may be located in complex terrains, making connection planning more intricate. The mathematical formulation is presented in Eqs. (1) to (9), with the corresponding nomenclature provided in Table 8 in Appendix B.

$$min \sum_{c \in \Omega^{Clu}} Length_c \tag{1}$$

where

$$Length_c = D(WT_i, WT_j)^2 \cdot Link(WT_i, WT_j) \tag{2}$$

$$D(WT_i, WT_j)^2 = (X_{WT_i} - X_{WT_j})^2 + (Y_{WT_i} - Y_{WT_j})^2 \tag{3}$$

s.to.

$$\sum_{j \in Clu_c} F_{i,j}^{Clu_c} \cdot AM(i,j) = \sum_{j \in Clu_c} F_{j,i}^{Clu_c} \cdot AM(j,i) + b_i^{Clu_c} \qquad \forall c \in \Omega^{Clu}, i \in Clu_c \tag{4}$$

$$b_i^{Clu_c} = \begin{cases} -1 & i \neq Start\ \ point\ \ inside\ \ Clu_c \\ card(Clu_c) - 1 & i = Start\ \ point\ \ inside\ \ Clu_c \end{cases} \tag{5}$$

$$M_c \cdot Link(WT_i, WT_j) \cdot AM(i,j) \geq F_{i,j}^{Clu_c} \cdot AM(i,j) \qquad \forall c \in \Omega^{Clu}, i,j \in Clu_c \tag{6}$$

$$0 \leq F_{i,j}^{Clu_c} \leq M_c \qquad \forall c \in \Omega^{Clu}, i,j \in Clu_c \tag{7}$$

$$Link(WT_i, WT_j) = Link(WT_j, WT_i) \qquad \forall c \in \Omega^{Clu}, i,j \in Clu_c \tag{8}$$

where

$$M_c = (card(Clu_c) - 1) \qquad \forall c \in \Omega^{Clu} \tag{9}$$

To reduce computational burden, this model is formulated as a mixed-integer linear program (MIP). The objective function aims to minimize the sum of the squares of the lengths of transmission cables connecting all WTs within each cluster, as presented in Eqs. (1) to (3). The decision variable $Link(WT_i, WT_j)$ in this model determines the connection status among the WTs within each cluster, with 1 indicating a connection and 0 indicating a disconnect. Eq. (4) imposes a constraint on balancing the net flow at each node, where the parameter $b_i^{Clu_c}$ depends on the selection of the start terminal, as illustrated in Eq. (5). Eqs. (6) and (7) define the bounds of the net flow within each cluster. Eq. (8) ensures the symmetry of the output of decision variables as the model processes all nodes.

The adjacency matrix, denoted AM, contains predetermined parameters that indicate the feasible connection status among the WTs. Each WT can only connect to neighboring WTs, with 1 indicating a possible connection and 0 indicating an absolute disconnection. In the OWF example with nine WTs shown in Fig. 4, WT_5 could be potentially connected to any of the other eight WTs, as indicated by 1 in the matrix AM. However, ultimately, it can only be connected to one of those eight WTs, and this final connection status is reflected in the variable $Link$. On the other hand, WT_1 could only be potentially connected to

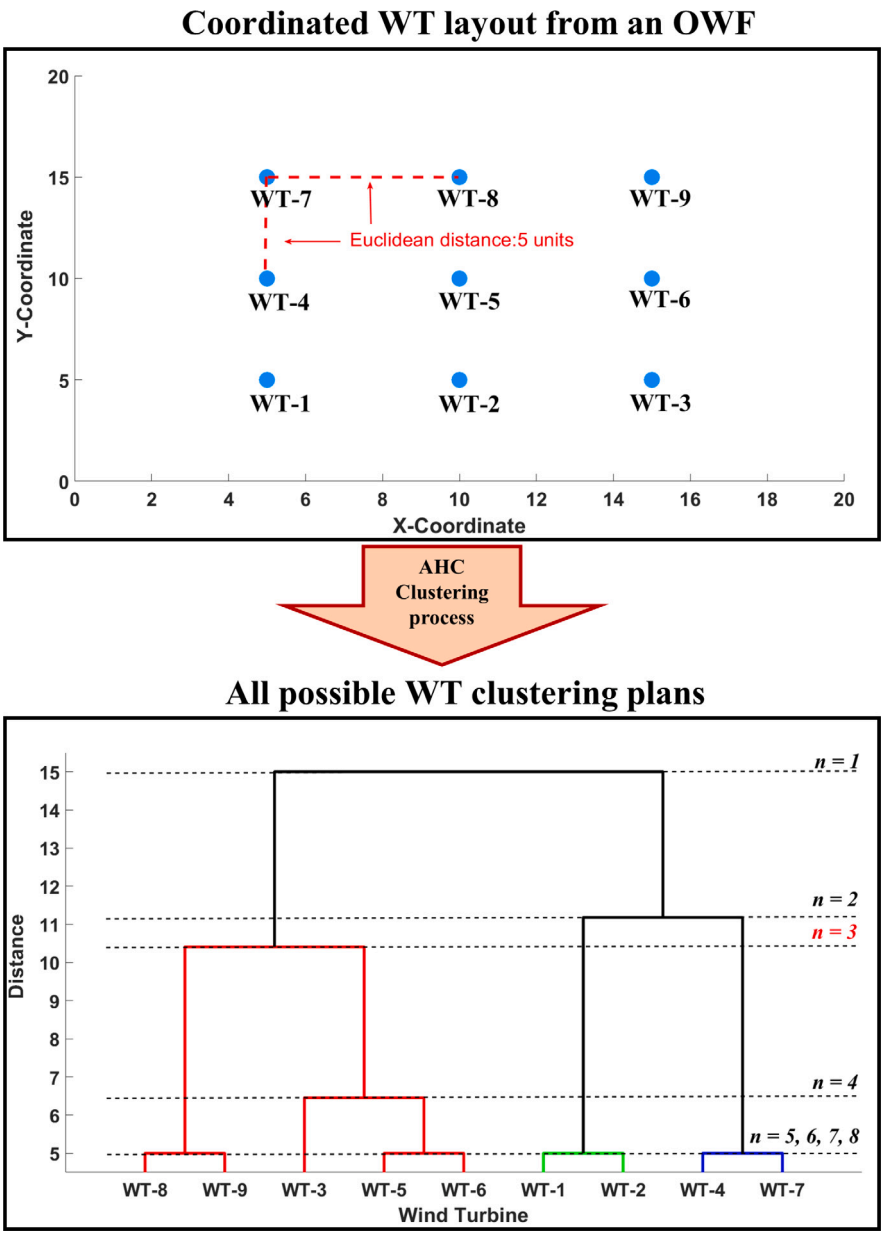

Fig. 4. Illustrative AHC process.

WT_2, WT_4, and WT_5, and it is absolutely prohibited to connect to other WTs, as indicated by 0 at the corresponding positions of the matrix AM.

Concerning the latter (optimal cluster planning model), the goal is to determine the location of SUB, where all clusters are aggregated and connected to OCP, while minimizing the total length (and total cost) of the main transmission cables. The optimal cluster planning model is presented in Eqs. (10) to (14), with the corresponding nomenclature provided in Table 9 in Appendix B.

$$min\ Cost_{transmission} = C^{Sub-Ocp} \cdot D(Sub, Ocp)^2 + C^{Clu-Sub} \cdot \sum_{c \in \Omega^{Clu}} \sum_{i \in Clu_c} \left[D(WT_i^c, Sub)^2 \cdot Link(WT_i^c, Sub) \right] \quad (10)$$

where

$$D(Sub, Ocp)^2 = (X_{Sub} - X_{Ocp})^2 + (Y_{Sub} - Y_{Ocp})^2 \quad (11)$$

$$D(WT_i^c, Sub)^2 = (X_{WT_i^c} - X_{Sub})^2 + (Y_{WT_i^c} - Y_{Sub})^2 \quad (12)$$

s.to.

$$\sum_{i \in Clu_c} Link(WT_i^c, Sub) = 1 \qquad \forall c \in \Omega^{Clu} \quad (13)$$

$$X_{Sub}\ ,\ Y_{Sub} \geq 0 \quad (14)$$

In Eq. (10), the objective function is formulated as the total cost of constructing the transmission cables that connect each cluster to the SUB and connect the SUB to the OCP. The length of the transmission cables is assumed to be the Euclidean distance between the respective destination points, as presented in Eqs. (11) and (12). This model is subject to the constraint that within each cluster, only one WT is selected as the point of connection with the SUB, as presented in Eq. (13). The binary variable $Link(WT_i^c, Sub)$ is used to determine the connection status of each WT with the SUB, with 1 indicating a connection and 0 indicating a disconnect.

Table 3
Definition of power curtailment severity.

System failure severity level	Power curtailment severity range
$Level_1$	(0%, 25%] of installed capacity at OWF
$Level_2$	(25%, 50%] of installed capacity at OWF
$Level_3$	(50%, 75%] of installed capacity at OWF
$Level_4$	(75%, 100%] of installed capacity at OWF

Table 4
Combination of fault occurrence time and degraded system duration.

Index	(Time, Duration)	Index	(Time, Duration)	Index	(Time, Duration)	Index	(Time, Duration)
Com_1	(0:00 a.m, 6 h)	Com_5	(6:00 a.m, 6 h)	Com_8	(12:00 p.m, 6 h)	Com_{10}	(18:00 p.m, 6 h)
Com_2	(0:00 a.m, 12 h)	Com_6	(6:00 a.m, 12 h)	Com_9	(12:00 p.m, 12 h)		
Com_3	(0:00 a.m, 18 h)	Com_7	(6:00 a.m, 18 h)				
Com_4	(0:00 a.m, 24 h)						

3.3. Scenario generation

The purpose of this study is to determine the optimal backup BESS capacity for OWFs to prepare for the impact of unexpected HILP contingencies. Constructing a valid scenario that captures the characteristics of HILP events and represents the resilience of OWFs is crucial to developing an optimal capacity decision-making model. Two key aspects require emphasis: (1) the results of HILP contingencies are more severe than those of other HPLI events, such as the failure of individual WT components or the sporadic distribution of failed turbines across the entire OWF; and (2) HILP events exhibit greater stochasticity in terms of their occurrence times and durations. To address these concerns, the definition of power curtailment severity and the integration of the time dimensions of the stochastic process of HILP events are presented in Tables 3 and 4, respectively.

In Table 3, the severity of the fault is defined as the proportional range of the affected generation capacity relative to the installed capacity at the OWF. This severity is categorized into four distinct levels. It should be noted that, in this study, failure of the entire cluster is considered the affected unit, rather than failure of a single WT. In other words, if the main transmission cable connecting the WT cluster to the SUB is disrupted, there is no way to deliver the energy generated in the impacted clusters to the OCP to meet the energy demand. Consequently, depending on the number of clusters, the total generation capacity of a WT cluster (or multiple clusters) needs to be aggregated to assess their suitability for the severity level of power curtailment when impacted by HILP events. A detailed mechanism for categorizing clusters into various levels is presented in Step #2 of the subsequent scenario generation framework, as illustrated in Fig. 5.

In Table 4, the time dimensions of stochasticity for HILP events encompass both the fault occurrence time and the duration during which the system experiences degraded operational conditions. These dimensions jointly capture the system's resilience performance, incorporating the interruption time and recovery period. The time scale used to model the HILP events in this study is 24 h, with an hour as the time step. To facilitate computational efficiency, four levels of fault occurrence time and degraded system duration are selected to represent the temporal stochasticity. The shortest power-curtailment duration is 6 h, while the longest is 24 h. As indicated in the table, there are a total of 10 different combinations of temporal scenarios. The integration of the severity of power curtailment with the time dimensions of the scenarios is illustrated in Step #3 of the scenario generation framework (Fig. 5).

By combining Tables 3 and 4, the authors of this work believe that this is the simplest and most straightforward approach to capture the severity characteristics of HILP events. This remains true even for the least severe power curtailment scenario, a 6-h power curtailment with a 25% loss of generation capability, emphasizing the significant impact of the proposed system failure scenario on the OWF's generation capability. Although a 6-h or even 24-h duration cannot fully capture post-disaster management for a transmission cable fault in reality, this assumption significantly reduces the computational burden and aligns with the scenarios mentioned in other studies [60,64]. Moreover, the proposed models are robust enough that the modeling timescale can be easily adjusted to any desired value, allowing the incorporation of real-world case parameters.

The scenario generation method proposed in this study consists of four main steps, as shown in Fig. 5, with the corresponding nomenclature in Table 10 in Appendix B.

The Step #1 involves reordering the WT clusters according to the total installed capacity of the incorporated WTs. Assuming a fixed clustering level, there are n WT clusters derived from the aforementioned AHC method, denoted as C_1, C_2, …, and C_n, with the corresponding total installed capacities denoted as $\sum_{i\in C_1}(Cap_i)^{Ins}$, $\sum_{i\in C_2}(Cap_i)^{Ins}$, …, and $\sum_{i\in C_n}(Cap_i)^{Ins}$, respectively. These clusters are then reordered into a sequence, where the WT cluster with the minimum total capacity is indicated as $Ord(1)$, and the WT cluster with the maximum total capacity is denoted as $Ord(n)$.

In Step #2, n WT groups are categorized into different severity levels of HILP power reduction, as defined in Table 3. Starting from the WT cluster $Ord(1)$ to the WT cluster $Ord(m)$, where $m \le n$, the clusters are included in the severity of system failure $Level_L$ if the installed capacities accumulated of these clusters satisfy both conditions presented in Eqs. (15) and (16). These conditions are checked iteratively for the four levels of severity of power curtailment until all n clusters are assigned to at least one severity level. Fig. 6 provides a simple example of five WT clusters to illustrate the process of categorizing affected WTs into each severity level.

$$25\% \cdot (L-1) \cdot Cap_{OWF}^{Ins} < \sum_{Ord(1)}^{Ord(m)} \sum_{i\in Cluster} (Cap_i)^{Ins} \le 25\% \cdot L \cdot Cap_{OWF}^{Ins} \tag{15}$$

$$25\% \cdot L \cdot Cap_{OWF}^{Ins} < \sum_{Ord(1)}^{Ord(m+1)} \sum_{i\in Cluster} (Cap_i)^{Ins} \tag{16}$$

In Step #3, the severity levels of the power cut are integrated with the time dimensions of the HILP contingencies, as described in Table 4. When the cluster number is fixed, there are 41 scenarios, including one scenario that represents normal operations without any impact from HILP events.

The final Step #4 involves assigning probabilities to each scenario. Scenario probabilities are determined on the assumption that events with more severe outcomes have lower probabilities, and vice versa. These probabilities are calculated by considering the ratio of the remaining generation capacities that still function properly for each scenario to the total remaining generation capacities in all scenarios.

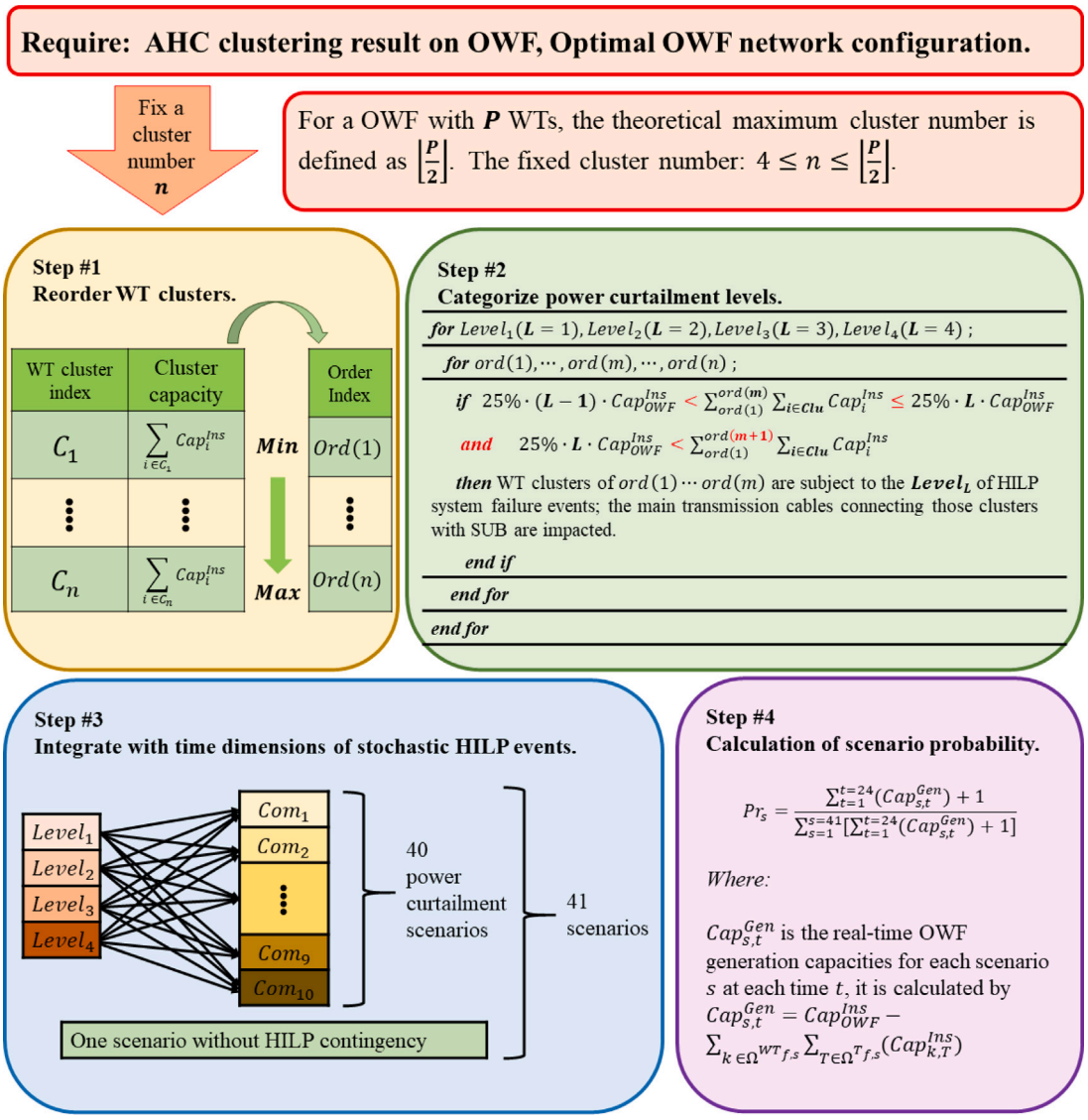

Fig. 5. Scenario generation framework.

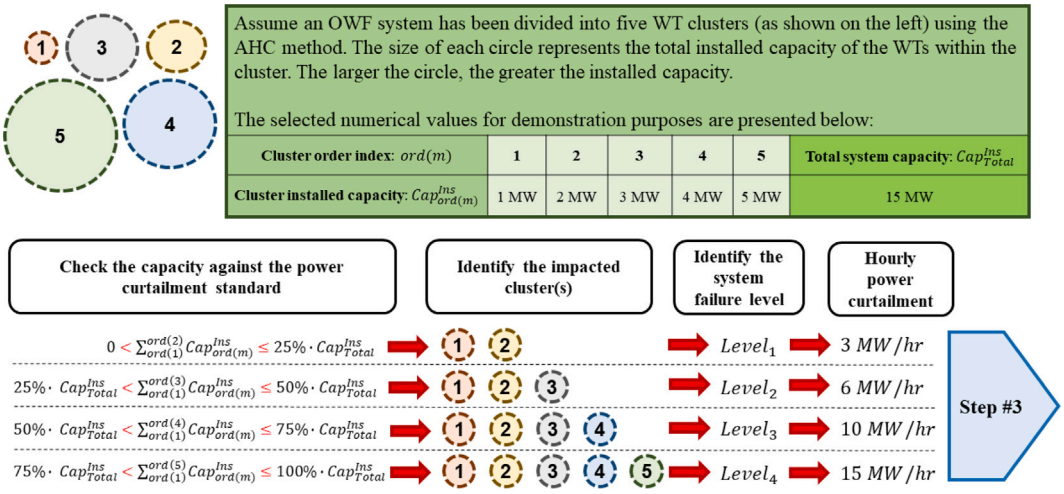

Fig. 6. Demonstration of power curtailment scenarios.

The mathematical form of this probability assignment is presented in Eq. (17), while Eq. (18) details the computation of the remaining generation capacity in real time that functions properly for the entire OWF in scenario s at each time t.

$$Pr_s = \frac{\sum_{t=1}^{t=24}(Cap_{s,t}^{Gen}) + 1}{\sum_{s=1}^{s=41}[\sum_{t=1}^{t=24}(Cap_{s,t}^{Gen}) + 1]} \qquad \forall s \in \Omega^{Scen} \tag{17}$$

where

$$Cap_{s,t}^{Gen} = Cap_{OWF}^{Ins} - \sum_{k \in \Omega^{WT_{f,s}}} \sum_{T \in \Omega^{T_{f,s}}} (Cap_{k,T}^{Ins}) \qquad \forall t \in \Omega^{Time}, s \in \Omega^{Scen} \tag{18}$$

and

$$\sum_{s \in \Omega^{Scen}} Pr_s = 1 \tag{19}$$

Three key points need to be emphasized regarding the assignment of probabilities. First, to ensure the positive characteristics of the probabilities assigned to all scenarios, the constant 1 is added to the real-time generation capacity in both the numerator and the denominator in Eq. (17). For example, in the scenario where the duration of the degraded system is 24 h, $\sum_{t=1}^{t=24}(Cap_{s,t}^{Gen})$ becomes zero. Without the inclusion of this constant in the formulation, the probability under this scenario would also be zero, which contradicts the validity of scenario construction. Second, the sum of probabilities from all scenarios equals 1, as illustrated in Eq. (19). Third, in Eq. (18), the remaining available generation capacity ($Cap_{s,t}^{Gen}$) is calculated by subtracting the total impacted WTs' capacity from the entire OWF system installed capacity (Cap_{OWF}^{Ins}). This calculation reflects the reduction in real-time generation capacity due to the degraded state of the system.

3.4. Optimal BESS capacity

The purpose of this model is to minimize the total resilience cost of planning the optimal capacity for a backup BESS while considering the system's resilience performance under the impact of HILP events. The objective function and related constraints are presented in Eqs. (20) to (30), with the definitions of parameters and variables utilized in this model listed in Table 11 in Appendix B.

$$\begin{aligned} &min\ \ Cost = C^{Ins} \cdot \overline{B} + \\ &C^{Rec} \cdot \sum_{s \in \Omega^{Scen}} \sum_{t \in \Omega^{Time}} Pr_s \cdot T_s^{fd} \cdot TL(Level_s)^f - \\ &C^{Rew} \cdot \sum_{s \in \Omega^{Scen}} \sum_{t \in \Omega^{Time}} Pr_s \cdot P_{s,t}^{Gen} \cdot \nabla_t \end{aligned} \tag{20}$$

s.to.

$$\begin{aligned} &B_{s,t} = B_{s,t-1} + SOC_{s,t} \cdot P_{s,t}^{Cha} \cdot \nabla_t \\ &- SOD_{s,t} \cdot B_{s,t-1}^{Discha} \qquad \forall t \in \Omega^{Time}, s \in \Omega^{Scen} \end{aligned} \tag{21}$$

$$\begin{aligned} &P_{s,t}^{Gen} \cdot \nabla_t - SOC_{s,t} \cdot P_{s,t}^{Cha} \cdot \nabla_t \\ &+ SOD_{s,t} \cdot B_{s,t-1}^{Discha} \geq De_t \qquad \forall t \in \Omega^{Time}, s \in \Omega^{Scen} \end{aligned} \tag{22}$$

$$SOC_{s,t} + SOD_{s,t} \leq 1 \qquad \forall t \in \Omega^{Time}, s \in \Omega^{Scen} \tag{23}$$

$$P_{s,t}^{Cha} \leq P_{s,t}^{Gen} \qquad \forall t \in \Omega^{Time}, s \in \Omega^{Scen} \tag{24}$$

$$B_{s,t}^{Discha} \leq B_{s,t} \qquad \forall t \in \Omega^{Time}, s \in \Omega^{Scen} \tag{25}$$

$$P_{s,t}^{Gen} \leq Cap_{s,t}^{Gen} \qquad \forall t \in \Omega^{Time}, s \in \Omega^{Scen} \tag{26}$$

$$\sum_{s \in \Omega^{Scen}} Pr_{s,t} \cdot B_{s,t} \leq \overline{B} \qquad \forall t \in \Omega^{Time} \tag{27}$$

$$B_{s,t=0} = Cap_{OWF}^{Ins} \cdot 24 \qquad \forall s \in \Omega^{Scen} \tag{28}$$

$$B_{s,t=24} \geq De_{t=1} \qquad \forall s \in \Omega^{Scen} \tag{29}$$

$$\overline{B}\ ,\ B_{s,t}\ ,\ B_{s,t}^{Discha}\ ,\ P_{s,t}^{Gen}\ ,\ P_{s,t}^{Cha} \geq 0 \qquad \forall t \in \Omega^{Time}, s \in \Omega^{Scen} \tag{30}$$

The objective function consists of three terms, as illustrated in Eq. (20). The first term calculates the capital cost of installing a backup BESS with a specific capacity $\overline{B}$. The second term computes the total system recovery cost required to restore the affected WT clusters to their normal state. This cost is influenced by the total length of the impacted transmission cables connecting the corresponding clusters to the SUB ($TL(Level_s)^f$), and it is assumed that it will increase with a longer duration of system restoration in a certain scenario of power reduction (T_s^{fd}). The third term incentivized energy storage in the battery, prioritizing the utilization of power generated by the WTs over the consumption of energy stored in the BESS. It can be interpreted in multiple ways. For example, it can be treated as income obtained from selling WT-generated electricity to energy consumers or as a financial reward applied to store more energy inside BESS. Regardless of the interpretation adopted, the ultimate goal is to ensure that sufficient energy is stored inside BESS to address unexpected system faults.

The battery operation constraint, as depicted in Eq. (21), defines the real-time energy stored in the battery. This energy storage depends on the (dis)charging state, the residual energy remaining in the battery from the previous time step (defined as $t-1$), and the power generation at the current time (denoted as t).

The energy balance constraint, as illustrated in Eq. (22), ensures that the total energy supply can meet the energy demand. The time step of this model is one hour ($\nabla_t = 1$ h), which facilitates a convenient conversion from the unit of power (kW) to the unit of energy (kWh). The energy supply sources are exclusively limited to the power generated by WTs ($P_{s,t}^{Gen}$) and/or the energy stored in the BESS from the previous time step ($B_{s,t-1}$), depending on the (dis)charging state. For example, when discharging is active, $SOD_{s,t}$ takes a value of 1, resulting in the charging state, $SOC_{s,t}$, being set to 0, according to the constraint presented in Eq. (23). In this scenario, both WTs and the BESS, specifically the energy discharged from the battery ($B_{s,t}^{Discha}$), collaborate to achieve the energy balance.

If the charging state is active, indicating that the power generated by the WTs caters sufficiently to energy consumers and can additionally supply surplus energy for storage in the BESS (denoted as $P_{s,t}^{Cha}$), it is entirely plausible that both $SOD_{s,t}$ and $SOC_{s,t}$ are inactive. This signifies that there is no need for the BESS to charge (or the full capacity is reached), while simultaneously ensuring that the power generated by the WTs is adequate to attain energy balance.

Although $P_{s,t}^{Cha}$ and $B_{s,t}^{Discha}$ are free variables in the model, they are constrained by their respective upper bounds, as presented in Eqs. (24) and (25), respectively. To be more specific, the total power charged into the battery at time t must not exceed the actual power generated by WT at that time ($P_{s,t}^{Cha}$), and the total energy discharged from the BESS at time t must not exceed the remaining energy from the previous time step ($B_{s,t-1}$). In other words, these two constraints limit the (dis)charging rate to no more than 1.

The constraint, as illustrated in Eq. (26), imposes restrictions on the real-time power generated from WTs when HILP events lead to the isolation of (some or even all) WT clusters, reducing the overall capacity available for electricity generation during the system degradation phase. The real-time generation capacity ($Cap_{s,t}^{Gen}$) is obtained from step #4 of the scenario generation process.

Eq. (27) establishes the relationship between the first-stage decision variables and the second-stage decision variables. For each time t, the real-time stored energy in the BESS, accumulated in the scenarios, must not exceed the planned BESS capacity, denoted as $\overline{B}$.

It is worth mentioning the significance of the initial and terminal battery energy conditions, as they play a crucial role in maintaining the feasibility of the proposed mixed-integer linear program. In this study, the initial stored energy in the BESS is assumed to be sufficiently large, allowing the program to begin even under the worst-case scenario of

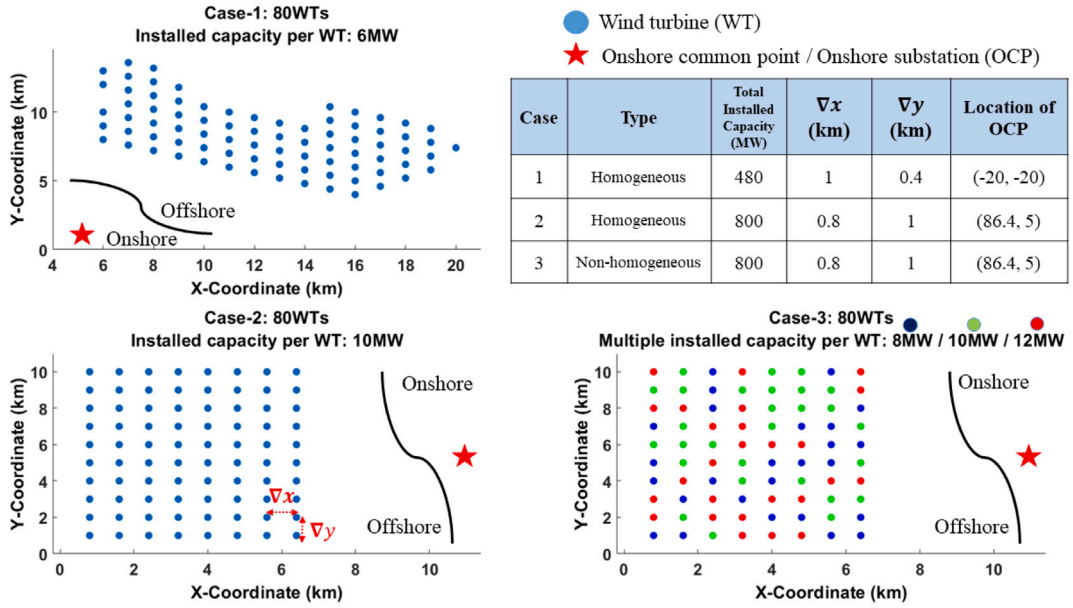

Case	Type	Total Installed Capacity (MW)	∇x (km)	∇y (km)	Location of OCP
1	Homogeneous	480	1	0.4	(-20, -20)
2	Homogeneous	800	0.8	1	(86.4, 5)
3	Non-homogeneous	800	0.8	1	(86.4, 5)

Fig. 7. Layout of test OWFs.

a 100% power outage occurring at the first time step for 24 h, as presented in Eq. (28). The terminal condition is designed to ensure that the stored battery energy at the end of the day is sufficient to meet the energy demand at the first time step, indicating that it has been prepared for use at the beginning of the following day, as presented in Eq. (29).

4. Test cases and data

In this study, three different OWFs are selected as test cases to verify the proposed methodology. The layout of the WTs and the location of the OCP have been visualized in Fig. 7. All WTs are evenly distributed geographically and have been placed in the Cartesian coordinate system accordingly. The distances between every two WT along the X axis and the Y axis, denoted ∇_x and ∇_y, respectively, are uniform.

The OWF in Case-1 is derived from a real OWF network called Banc de Guérance, which was constructed in France in 2015 [65]. It comprises WTs, each with an installed capacity of 6 MW. In Case-2 and Case-3, both cases represent OWFs consisting of 80 WTs located in the vicinity of research platforms in the North and Baltic Seas (FINO3), located 80 km west of the German island of Sylt [66]. The primary distinction between Case-2 and Case-3 is that in Case-2, the WTs have homogeneous individual installed capacities, while in Case-3, the WTs are nonhomogeneous, featuring three different levels of installed capacities and being randomly distributed within the network (26 WTs with 8 MW, 28 WTs with 10 MW, and 26 WTs with 12 MW).

Adopting these three distinct OWFs is advantageous for conducting a comparative study. The comparative assessment of system performance between Cases 1 and 2 is valuable in examining the influence of different WT layouts on the optimal BESS capacity. The comparison between Cases 2 and 3 aims to investigate the impact of unbalanced generation capacities within OWFs on the decision-making process to determine the optimal BESS capacity. Although wind speed and wake effects are not directly considered in this study, the design of Case-3 also seeks to account for these external uncertainties that lead to varying WT generation capacities.

Fig. 8 shows the hourly energy demand of end users onshore, which can only be supplied by OWF and BESS within the context of this study, represented as a percentage of the installed capacity of OWF over a 24-h period. These demand data represent the average of the complete demand data sample provided in a study that constructed a benchmark test system for network microgrids [67]. For reference purposes, the complete demand data is also provided in Appendix A of this study (Table 7). This demand change curve will be applied to all three OWF cases.

Several cost-related parameters in the model need to be assigned values. In the optimal OWF configuration model, three different types of transmission cables are used: the cable connecting the WT, the cable connecting the WT clusters to the SUB and the cable connecting the SUB to the OCP. The total transmission cost depends not only on the required cable length but also closely relates to the type of cables used for different purposes. In this study, the first two types adopt 50-HZ alternating-current (AC) transmission cables, while the last type uses high-voltage direct current (HVDC) cables. The appendix in the study [68] provides a complete selection of transmission cables with the corresponding unit costs. The reference values selected for the case study are presented in Table 5. Considering that the total installed capacity of the Case-1 network is smaller than that of Case-2 and Case-3, the transmission cables used for Case-1 are thinner than those used for Case-2 and Case-3, resulting in lower corresponding unit costs. Furthermore, it is expected that the sizes of the transmission cables within each WT cluster will vary, with the thickness of the transmission cable increasing as it approaches the connection point connected to the SUB. However, this study does not consider these differentiated characteristics of transmission cables within WT clusters for two reasons: (1) regardless of how the cluster network is configured, as long as the total length of transmission cable remains the same, the total cost of transmission cable inside the cluster remains the same, and (2) the transmission cost inside the WT cluster does not necessarily impact the research question in this study.

In the optimal BESS capacity model, three cost-related parameters are also considered: the unit capital cost for BESS, the unit cost for system restoration, and the unit incentives for prioritizing the use of energy generated from WTs instead of the consumption of energy stored in BESS. This model integrates both the planning phase and the operational phase. To avoid dominance of the parameters of the planning phase, the Levelized Cost of Electricity (LCOE) is selected for the planning phase parameters. First, utility-scale lithium ion batteries are chosen as the technology for BESS due to their yearly declining LCOE, with the most recent reference data indicating $150 per megawatt hour [69,70]. Second, assessing the unit cost for system restoration is challenging as it encompasses both human-based support management

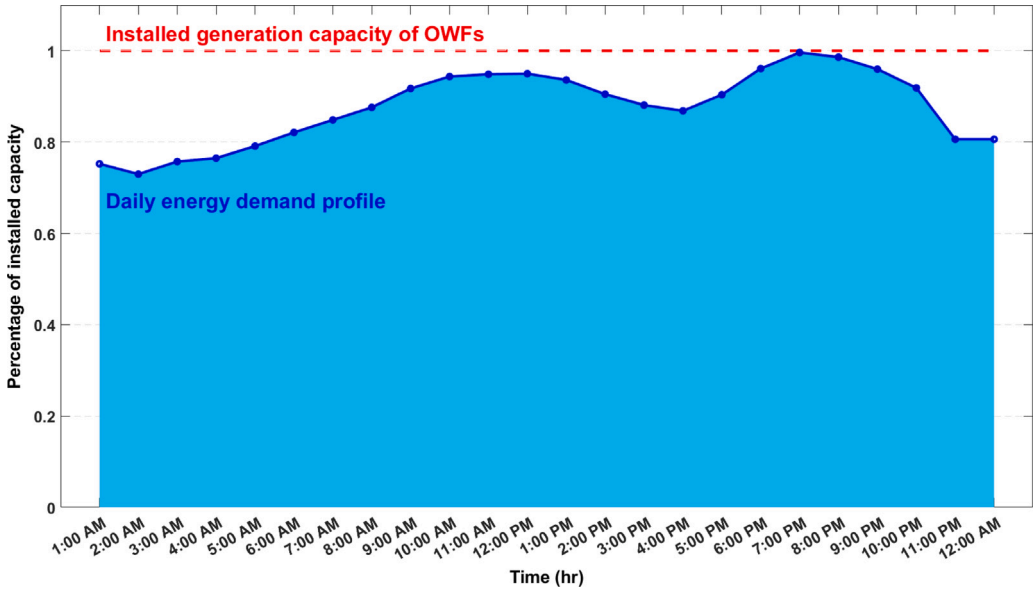

Fig. 8. Hourly energy demand profile.

Table 5
Value for cost-related parameters..

Parameter	C^{WT-WT} [68] (k$/km)	$C^{Clu-Sub}$ [68] (k$/km)	$C^{Sub-Ocp}$ [68] (k$/km)	C^{Ins} [69,70] ($/MWh)	C^{Rec} [21] ($/km h)	C^{Rew} [71,72] ($/kWh)
Technology	50HZ-AC	50HZ-AC	HVDC	Lithium-ion	–	–
Case-1	1600	2251	1424	150	2025.64	0.1512
Case-2 & Case-3	2089	2659	1755	150	2025.64	0.1512

costs and technical restoration strategies. The study in [21] provides a variety of post-disaster maintenance support strategies for OWFs. It concludes that the most cost-effective strategy involves providing the maintenance team with offshore accommodation, 24/7 work shifts, and the availability of helicopters and crew transfer vessels, resulting in a total cost of €16.4M/year. This figure can be converted to approximately $2025.64/h. Considering the time dimension of post-disaster scenarios in this study, a new unit is introduced to this parameter: the unit system restoration cost per main transmission cable length (km) per hour (h). This unit reflects that the longer the impacted main transmission cable (connecting WT clusters to the SUB) and the longer the degraded system period, the higher the system restoration cost. Third, in relation to the financial incentive to conserve energy within BESS, the average electricity price for the residential sector in the year 2022, 15.12 cents/kWh [71,72], is adopted as the value of this parameter. The reference values selected in this study are also listed in Table 5.

5. Results and discussion

In terms of specific modeling platforms, the AHC method and the stochastic scenario generation method are performed using MATLAB (R2022b version). The *Linkage* function embedded in Matlab offers great convenience in realizing the AHC method [73]. The minimum spanning tree model, the optimal clustering planning model, and the optimal BESS capacity model are implemented using the AMPL (A Mathematical Programming Language) modeling platform, utilizing Gurobi, Bonmin, and Gurobi solvers, respectively. The simulation is conducted on a machine equipped with an Intel(R) Core(TM) i7-7700 CPU @ 3.60 GHz and 16 GB of RAM.

The results are presented in the following sequence: first, the visualization of the optimal BESS capacity profile; second, an elucidation of the significant number of clusters; third, a discussion of the optimal cluster number; fourth, a sensitivity analysis of cost-related parameters on the proposed optimization model; and fifth, a validation of the proposed scenario generation method is conducted based on a comparison of modeling outputs from different system failure time-dimension settings.

In addition, it is worth mentioning the numerical probabilities assigned to each scenario during the modeling process. When examining the numerical probabilities across 41 scenarios, two key points need to be highlighted. Firstly, the difference in numerical probabilities is very small; the highest probability (non-fault scenario) is only 3.5%, and the lowest probability (most severe blackout scenario) is below 0.1%. The probability distribution of all other scenarios exhibits a monotonic trend within this range (with more severe power-curtailment outcomes having lower probabilities of occurrence). Secondly, these numerical observations are sufficient to justify that all scenarios are treated relatively fairly, eliminating the situation where the entire scenario is biased toward one with a superlarge probability. Combined with the previous comments on the severity of proposed power curtailment scenarios in Section 3.3, this evidence jointly corresponds to the concept that all scenarios are characterized by the "Low-Probability" but "High-Impact" principle.

5.1. Profiles of optimal capacity

The optimal BESS capacity profiles, presented as the ratio of optimal capacity to daily electricity generation at full capacity of the entire OWF without considering the capacity factor, are displayed as blue dots in Fig. 9. Simultaneously, the values of the objective function (total resilience cost) from the optimal BESS capacity model under corresponding clustering level are highlighted as red lines in Fig. 9.

As the number of clusters increases, the total cost profile shows an upward trend. This is primarily due to the additional costs incurred when a greater number of cluster transmission cables are affected by HILP events and require rehabilitation. However, optimal BESS capacity profiles will eventually stabilize or converge within a narrow

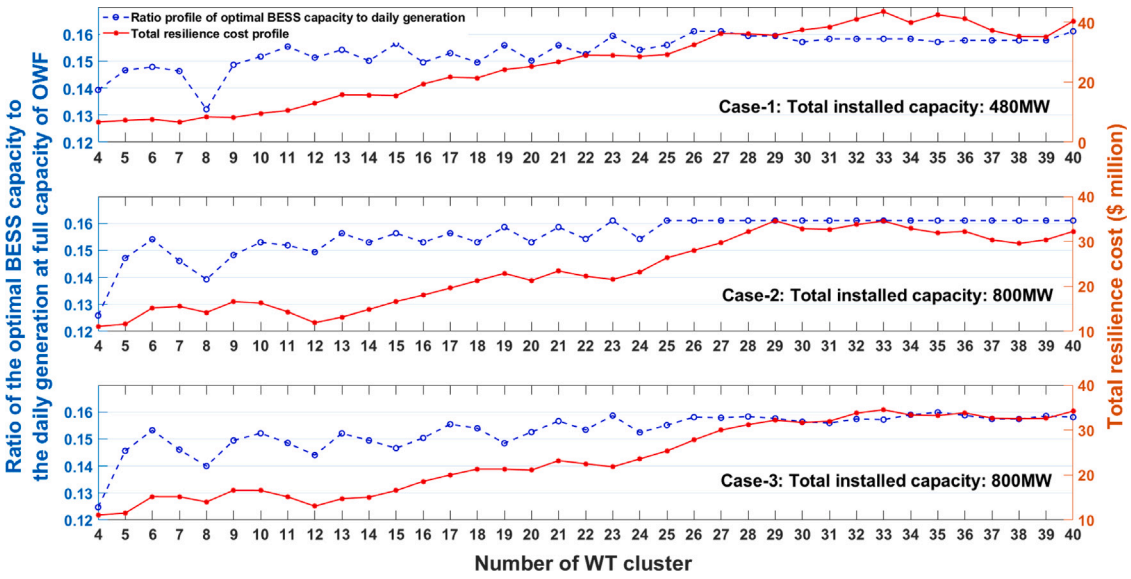

Fig. 9. Profiles of optimal backup battery capacities and total resilience cost.

range of numerical variations. By comparing the profiles across the three test OWFs, a crucial observation can be detected: the optimal BESS capacity is approximately 16% of the daily electricity generation at the full capacity of the OWF (without considering the capacity factor). The capacity factor of the OWF is not included in the proposed modeling process, yet the observed result can be readily and validly generalized. That is, for an OWF with a capacity factor indicated by *c.f*, the optimal BESS capacity is $(\frac{16\%}{c.f})$ of the daily generation at full capacity. For example, the average global capacity factor of OWFs is 42% [74], indicating that the optimal BESS capacity should be 38% of the daily generation at full capacity.

5.2. Significant number of cluster

For each OWF case, a significant number of clusters can be identified in Fig. 9. Beyond this significant number, the profiles of optimal BESS capacities are treated as stabilized, and the total cost at this point reaches a relatively (local) minimal value. For example, in Case-1, a cluster number of 29 can be considered significant, while in Case-2, a cluster number of 25 serves as a significant threshold. In Case-3, the significant cluster number is 26. To improve clarity, Fig. 10 presents a comparison of the dispersion of optimal BESS capacities under all cluster conditions and the stabilization phases for all OWF cases.

Considering the characteristics of different OWFs, it is crucial to highlight three important points regarding the validity of the proposed modeling methodology. First, the proposed model effectively captures the true optimal BESS capacity profile, as it demonstrates a consistent convergent variation trend regardless of the installed capacities of the OWF. Second, when comparing the results between Case-1 and Case-2, it is evident that the optimal BESS profile achieves a better convergence when the WT layout is coordinated, in contrast to cases where the WT layout is scattered. Third, a comparison between Case-2 and Case-3 reveals that the optimal BESS profile exhibits stronger convergence when all WTs have homogeneous installed capacities. This phenomenon may be attributed to environmental uncertainties, such as wind speed, which can negatively affect the decision-making process for the optimal BESS capacity (Case-3). However, despite these challenges, the convergent trends observed in all cases validate the robustness of the proposed modeling methodology.

The conceptual and alternative practical OWF configurations for each test case, under the significant number of clusters, are presented in Fig. 11. There are three points worth discussing with respect to OWF configurations. First, a significant number of clusters does not necessarily correspond to the optimal cluster number for OWF configurations in practice. Although a significant number of clusters provides valuable information on determining optimal BESS capacities using the proposed methodology, it is entirely possible to configure the OWF structure with an optimal cluster number that differs from this significant number of clusters while still installing the optimal BESS capacities obtained from the modeling process.

Second, the configuration within each cluster is determined using the minimum spanning tree algorithm, with the primary objective being the minimization of transmission length (and associated costs). Actually, this study considers all possible configurations, the cost-minimizing outcomes happen to be the radial topologies. Nonetheless, there are alternative layout structure options that aim to improve system operational reliability, but these are beyond the scope of this research study. However, the configurations within each cluster, as shown in Fig. 11, are not unique and can be adjusted to improve reliability, although at the expense of a higher investment cost. This trade-off is demonstrated in Fig. 12, where the meshed layout for the WT cluster is shown to be more reliable, as discussed in [42].

Third, the presence of crossing transmission lines in the conceptual configuration subfigure in Fig. 11 is easily noticeable. One of the assumptions in the optimal OWF topology modeling step is that cable crossings are allowed to simplify the computational burden of the algorithms, and Euclidean distances are used to represent the length of transmission cables. As stated previously, this study does not aim to optimize the OWF topology for resilience enhancement, but rather to explore the impact of various OWF configurations on decision-making regarding optimal BESS capacities. Therefore, the assumption of allowing cable crossings facilitates capturing a complete spectrum of OWF configurations, from the fewest to the greatest number of clusters. This assumption is also supported by the previous study [43]. However, in practical applications, the layout of actual transmission cables is more flexible, as illustrated on the right side of Fig. 11, allowing for adjustments in path selection and installation methods without cable crossing. This approach was also deemed acceptable in the research study [43].

5.3. Optimal cluster number

As mentioned previously, the significant number of clusters does not necessarily equal the optimal cluster number for OWFs. In practice,

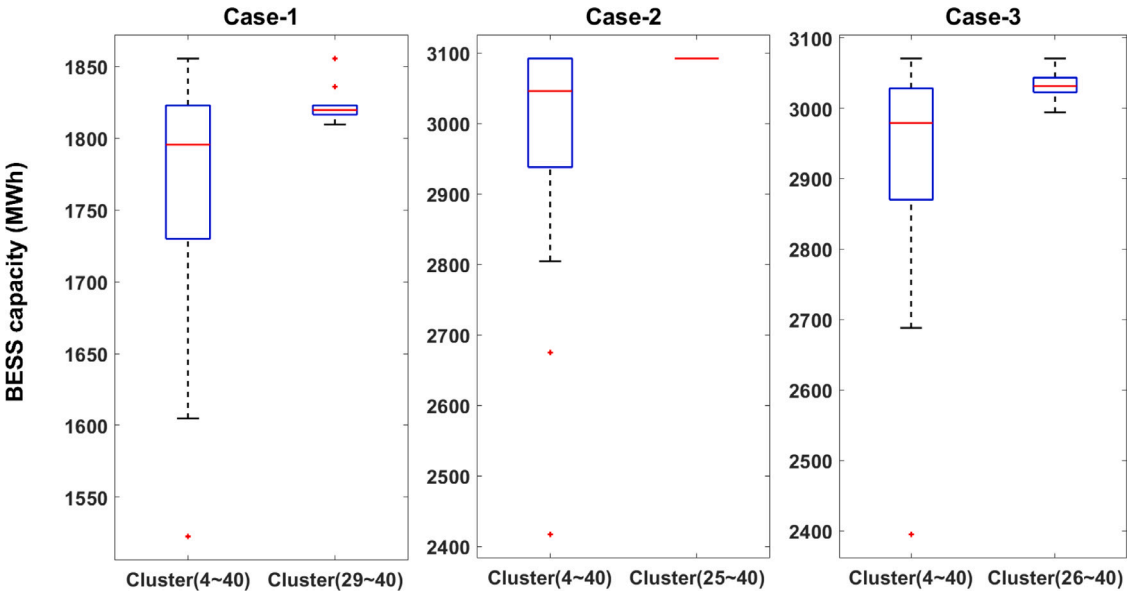

Fig. 10. Distribution of optimal capacities.

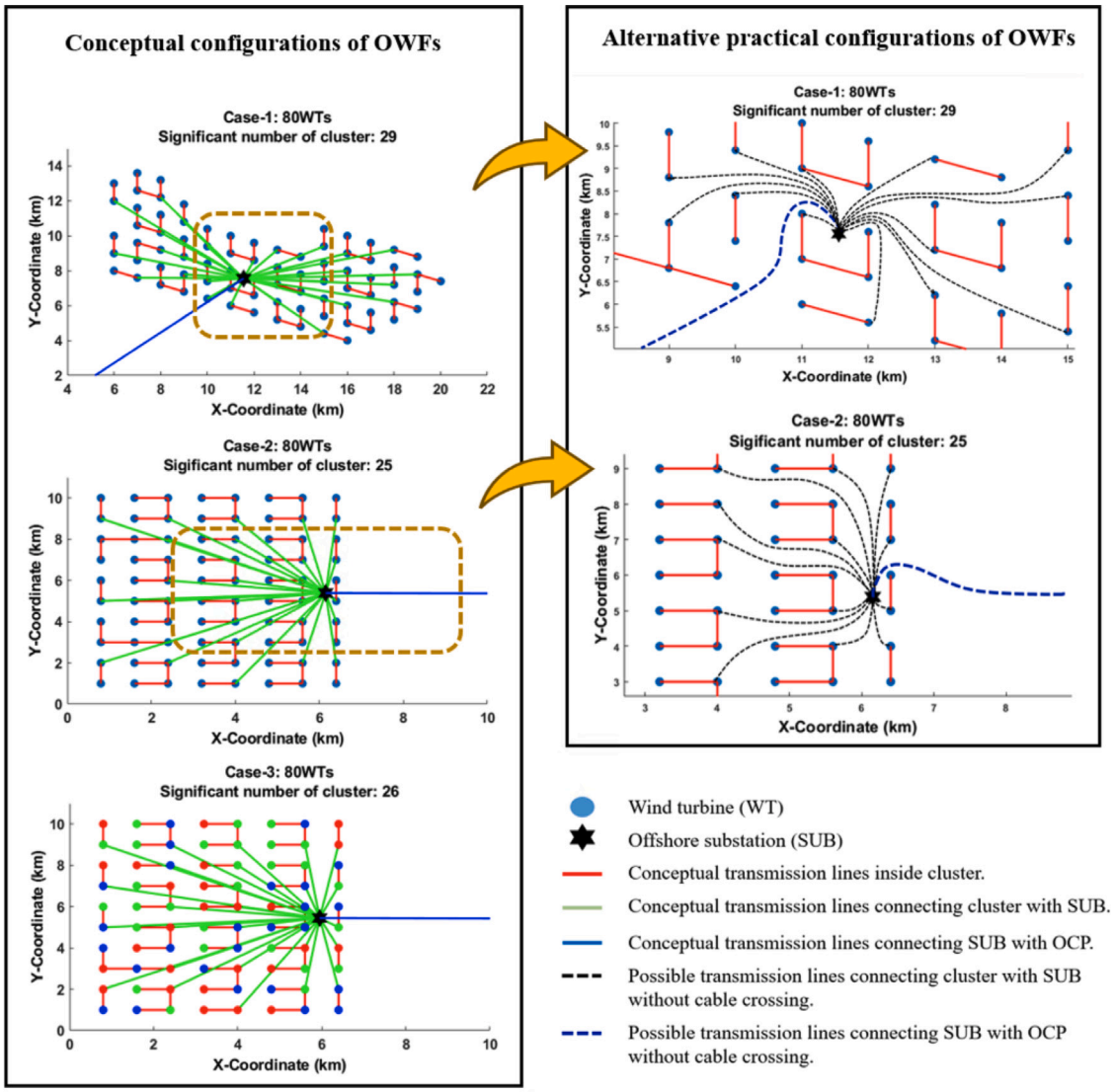

Fig. 11. Conceptual and alternative practical OWF configurations under the significant number of clusters.

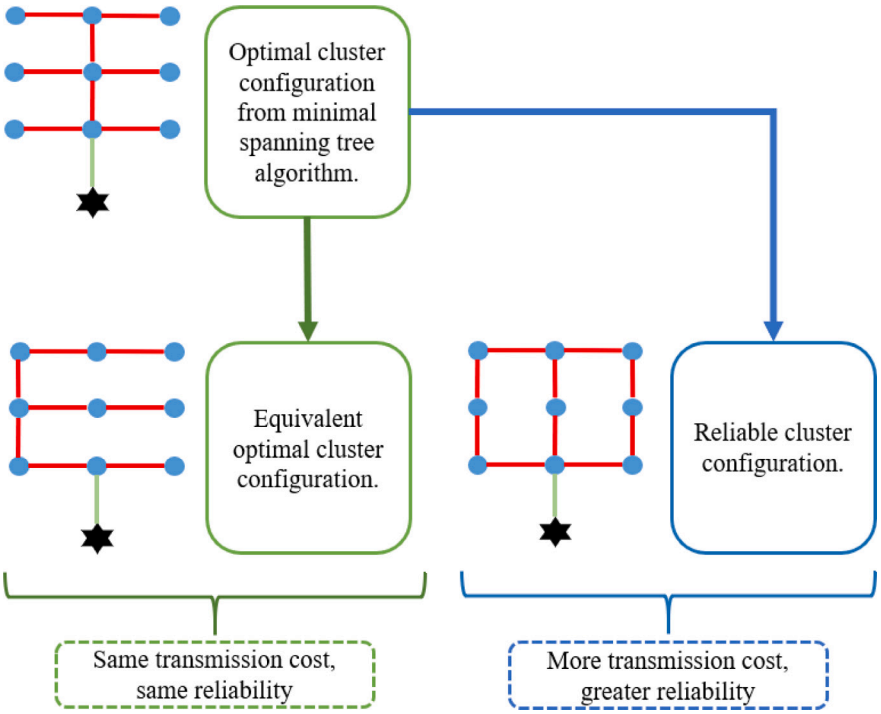

Fig. 12. Cluster configuration adjustment.

the optimal cluster number can be determined by considering both the WT layout and the maximum transmission cable capacity. Specifically, the capacity of the transmission cable imposes an upper limit on the power generated from the entire WT cluster, resulting in a predetermined minimum number of WT clusters for the entire OWF. Once the minimum number of clusters is established, classical clustering criteria can be used to evaluate the optimal number of clusters based on the geographical layout of the WTs. As clarified in Section 3.1, in this study, the minimum number of clusters for all test OWFs is set at $n = 4$ (because there are four power curtailment severity levels), indicating the utilization of the maximum capacity of transmission cables under that scenario. It should be noted that, to present a broader spectrum of optimal BESS capacity profiles at various clustering levels, this study does not consider specific transmission cable capacities as decision variables. However, addressing this aspect in future studies can contribute to practical improvements in the proposed model.

The optimal cluster number can also be theoretically determined by employing graph theory and comparing total transmission cable costs. Fig. 13 provides a visual representation of the optimal cluster number based on three classical clustering methods: Elbow method, gap statistic method, and Silhouette method [75]. Furthermore, Fig. 14 visually represents the total transmission cable costs profiles for all OWFs in this study.

In Fig. 13, the optimal cluster numbers for OWFs using different clustering methodologies are indicated by arrow icons. The Elbow method identifies the optimal cluster when a threshold is reached, while the gap statistic method identifies it when the gap statistic is at its highest. The silhouette method, on the other hand, determines the optimal cluster number when the silhouette value reaches its peak. It should be noted that the optimal cluster size for each OWF is considerably smaller than the significant number of clusters identified in previous discussions. For clarity, if the transmission cable capacity were introduced as a constraint in the model, as the maximum transmission cable capacity decreases, the spectrum of valid clustering profiles would narrow. This could potentially lead to a change in the optimal cluster number for configuring OWFs.

In Fig. 14, it is evident that the total cost of the transmission cable within the WT cluster (*i.e.*, connecting the WTs) is numerically lower than the total cost of the transmission cable outside the WT cluster (*i.e.*, connecting the WT cluster to the SUB and connecting the SUB to the OCP). This indicates that the total cost of the transmission cable is primarily influenced by the cost of the transmission cable outside the WT cluster. Similarly, this numerical comparison validates that there is no need to emphasize the network configuration within the WT cluster for this study, aligning with the assumption mentioned in Section 4.

5.4. Sensitivity analysis

To validate the proposed optimal BESS capacity model, a sensitivity analysis was performed to assess the influence of variations in cost-related parameters on the optimal BESS capacity and the corresponding total resilience cost. This sensitivity analysis is specifically applied to Case-1, within the context of its significant number of clusters, as defined in Section 5.2.

The results of the sensitivity analysis verify the robustness of the proposed optimal BESS capacity model in determining the optimal BESS capacity, as illustrated in Fig. 15, where variations in cost-related parameters do not significantly influence the output of the optimal decision variable. In terms of the total resilience cost, it is more sensitive to the unit post-disaster recovery cost, but not dominated by the BESS LCOE and the unit incentives parameter. From an optimization perspective, research on optimizing post-disaster system restoration costs is a topic of future interest, but it does not inherently impact the decision-making process regarding optimal BESS capacity.

5.5. Validity of scenario generation

The time dimensions of the stochasticity for HILP contingencies in this study are other important factors that influence the optimization model. These dimensions not only determine the computational size of the model, but also affect the probabilities assigned to system failure scenarios under varying severity levels. Consequently, a comparison of the results of the modeling under different time dimensions has been made based on Case-2, with the alternative time dimension parameters presented in Table 6. The BESS profiles in different system failure

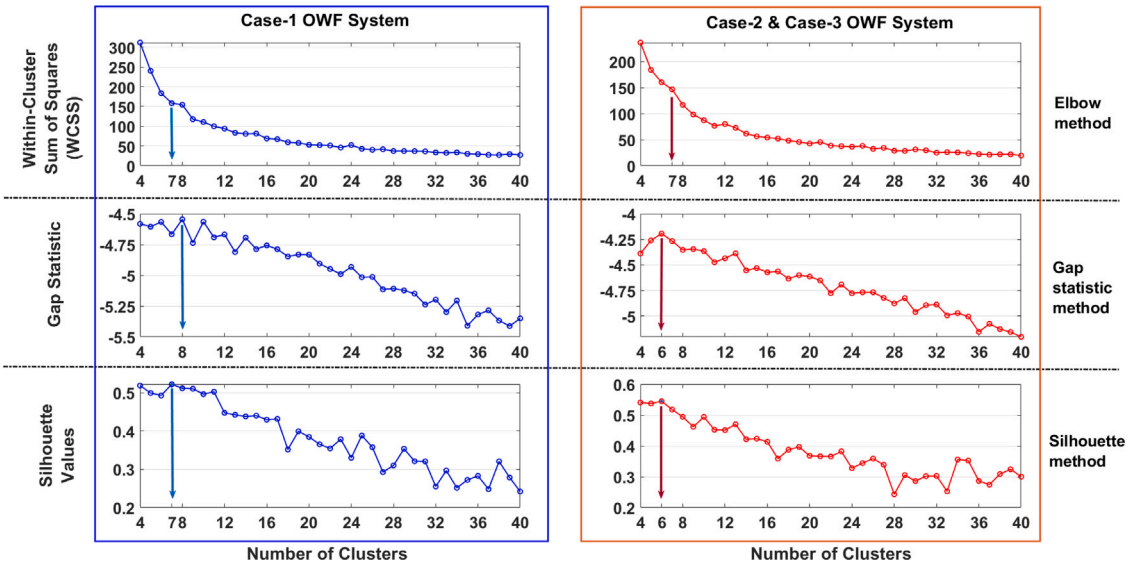

Fig. 13. Comparison of optimal cluster number under different methods.

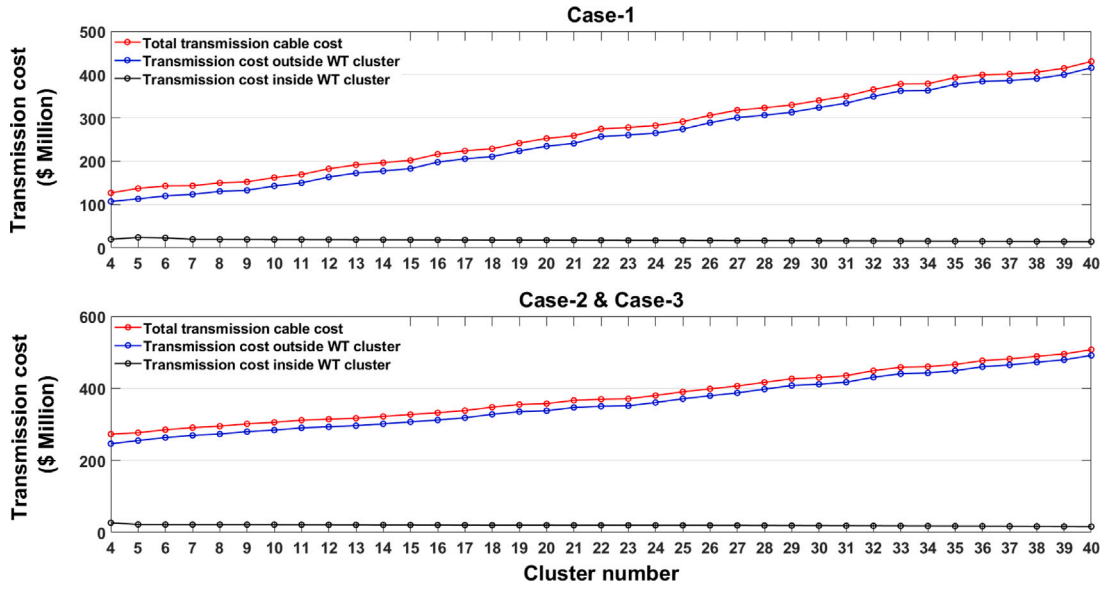

Fig. 14. Total transmission cable cost.

Table 6
Modifications in alternative system failure scenario generation.

Scenario	Original	Alternative-1	Alternative-2
Modeling duration	24 h	24 h	48 h
Shortest system failure period	6 h	3 h	6 h
Total number of scenarios	41	145	145
Daily power generation at full capacity	19 200 MWh (800 MW × 24 h)	19 200 MWh (800 MW × 24 h)	38 400 MWh (800 MW × 48 h)

scenarios are presented in Fig. 16. As illustrated, the numerical values of the BESS profiles in alternative scenarios deviate from those in the original scenario. However, the trend of variation remains consistent, as the profiles converge beyond the same number of clusters.

It is necessary to justify these numerical variations under different scenarios of system failure time dimensions. In two-stage stochastic programming with recourse, the first-stage decision variables are largely independent of the uncertainties in the second-stage variables. In this study, second-stage scenarios are characterized by uncertainties in the occurrence and duration of HILP contingencies. The probabilities associated with each second-stage uncertainty scenario play a crucial role in determining the optimal first-stage decision variables. Fig. 17 illustrates the comparison of probability distributions for system failure scenarios across different settings of time dimension. The upper plots show the number of scenarios categorized into each range of severity of the power cut and the accumulated probability of all scenarios within each category. The lower plots show the distribution of numerical probabilities for scenarios within each category of power restriction.

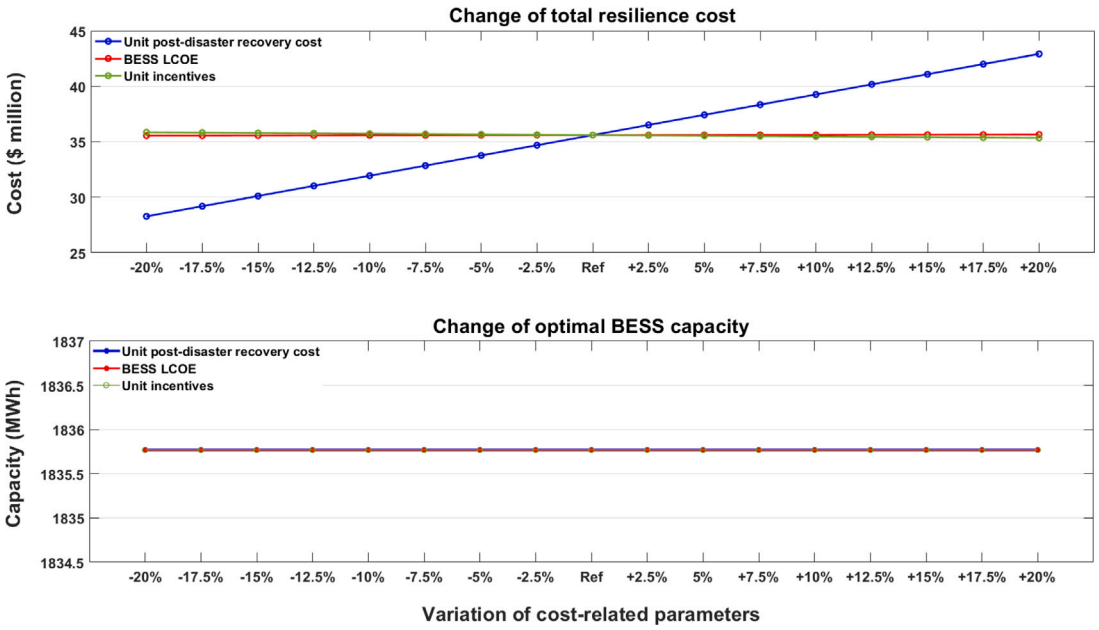

Fig. 15. Sensitivity analysis under the significant number of cluster of Case-1.

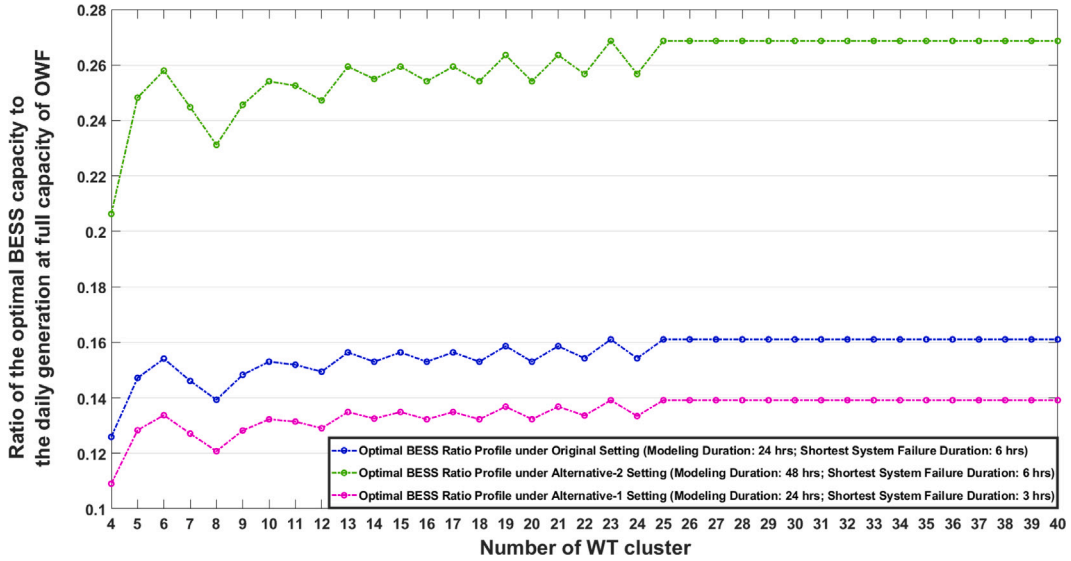

Fig. 16. Comparison of optimal BESS profiles under different system failure scenarios (Demonstration for Case-2).

One of the assumptions for scenario generation is that more severe system failures have lower failure probabilities. As illustrated in the plots on the bottom row, this assumption is confirmed across all conditions, with probabilities for scenarios involving greater power curtailment decreasing regardless of the time-dimension settings. However, as the shortest system failure duration decreases (Alternative-1) or the overall modeling duration is extended (Alternative-2), the number of less severe scenarios increases, leading to a skew and bias in the overall uncertainties toward less severe scenarios. In contrast, in the original scenario generation setting, the number of scenarios in different power curtailment ranges remains relatively unbiased, mitigating the risk of bias in the ultimate optimal values.

Furthermore, when the modeling duration is extended to 48 h, as demonstrated in Alternative-2, scenarios with a longer failure duration require that the BESS capacity be sufficient to meet the power demand over the extended period. Consequently, this results in higher ultimate values compared to the original setting, albeit at the cost of increased economic investment in larger BESS capacities. Hence, it is still appropriate to adopt the original scenario generation setting, as it helps mitigate biased modeling outputs. Furthermore, the modeling methodology used in this study is robust, as the ultimate BESS profiles converge in a consistent pattern. The specific parameter settings depend on stakeholders' estimations of practical OWF situations and the power demands that have to be satisfied.

6. Summary and conclusions

In this study, a sequential "planning + operational" model is proposed to investigate the influence of the optimal network topology on determining the optimal BESS capacity for independent OWFs. The objective is to improve the resilience of the system in the face of HILP events that cause short- to medium-term outages. The planning phase includes an AHC approach that illustrates all clustering levels and an optimal OWF configuration model under each clustering level.

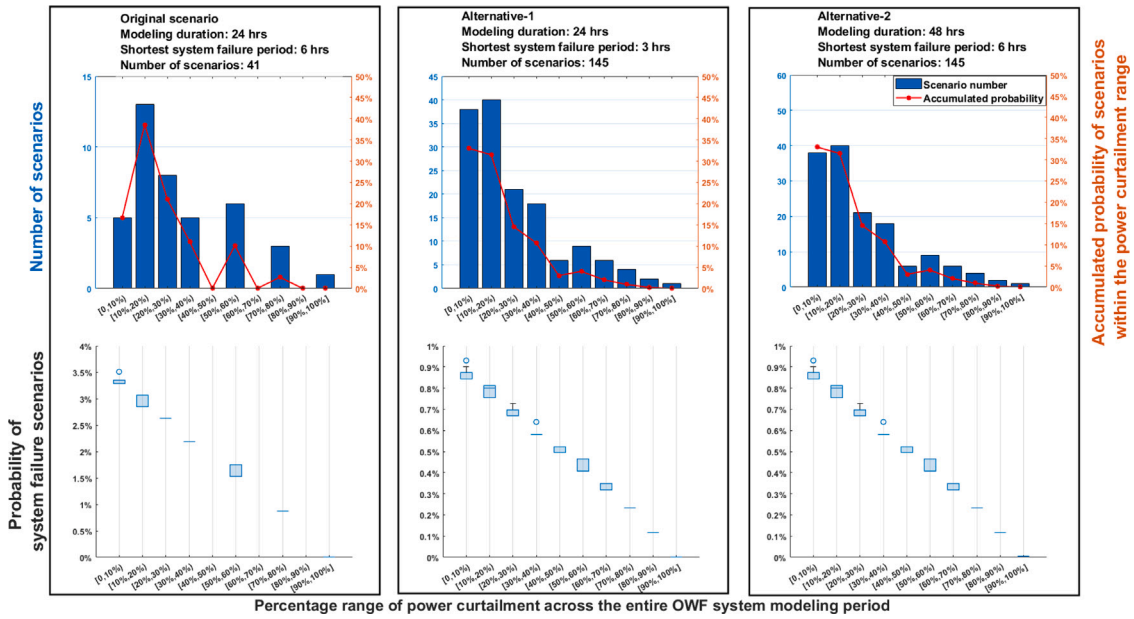

Fig. 17. Comparison of system failure probability across different failure time dimensions (Demonstration for Case-2 under significant number of cluster conditions).

Within this phase, the network configuration within clusters and the aggregation of clusters to SUB are treated as two independent modeling sectors. Once the optimal network topology is fixed under a given cluster number, stochastic power curtailment scenarios are generated by assuming the disconnect of the main transmission cables connecting the WT clusters with the SUB, resulting in a degraded power generation period. In this scenario, the optimal BESS capacity model is implemented to determine the BESS capacity while minimizing the total resilience cost as the main operational target.

For each distinct OWF, the optimal BESS capacity varies in correspondence with different clustering levels. However, the eventual convergence of the BESS profiles remains consistent between different test systems as the size of the WT clusters decreases. This consistent trend verifies the validity of the proposed model. They also illustrate the ultimate convergent profile of BESS capacities as the size of WT clusters decreases. This marks the existence of an optimal BESS capacity (approximately 16% of the daily electricity generation at full capacity without considering the capacity factor in the context of the modeling settings in this study) for the OWFs in various configuration circumstances, thus enhancing the resilience of the system. The sensitivity analysis of cost-related uncertainties in the modeling results, along with the comparison of outcomes under different time-dimension settings, verifies the robustness of the optimization model and the scenario generation method, further consolidating the generalizability of the proposed modeling approach.

Clarifying the difference between the significant number of clusters identified and the optimal number of clusters provides valuable information to system planners and operators. Although the significant number of clusters marks the optimal BESS capacity, OWFs do not necessarily have to be constructed under that clustering level. Instead, several other criteria are considered to determine the optimal cluster number, such as WT layout, evaluation of transmission cable costs, and reliability evaluation of different network topologies within each cluster, among others. However, in the event of contingencies, OWFs may undergo system reconfiguration to isolate affected zones and reduce cascading impacts. In such cases, the optimal BESS capacity derived from the proposed modeling remains unaffected by system reconfiguration, further confirming the validity of the results.

This study also offers several practical and managerial insights for system planners and policymakers. For system planners, recognizing the role of energy storage in expanding renewable-based generation technologies is essential for sustainable development, both technically and economically. Energy storage systems can be shared among different generation sources, jointly providing energy to end-users via the grid and enhancing the resilience of the entire integrated energy system. For policymakers, it is imperative to enact the right instruments to support the installation of optimal energy storage capacity that is crucial to stabilizing the electricity market with higher renewable penetration. This includes allowing negative pricing strategies to manage excessive energy output and promoting adaptive day-ahead market designs between renewable-based utilities and conventional utilities that still supply most of energy to end-users.

Undeniably, there is no consensus on the definition and specific quantification of the resilience of the system [76]. In our study, the duration of the system failure is used as a simplified metric that encompasses all four stages of the resilience process to create scenarios of energy supply shortages. Depending on different research objectives, researchers can focus on one of these phases or treat the entire resilience process as a unified whole. Our study adopts the latter approach. However, once the optimal BESS capacity profile is identified, our research could be further expanded to investigate the specific regulation of BESS energy usage during the system restoration phase only. This regulation could also be influenced by the coordination of other available power generation technologies, BESS installation locations, and modifications to the management of the electricity market during emergencies [77]. Furthermore, considering various aspects of the installation of a utility-scale BESS, such as environmental impacts, including ecological footprint, recycling, and disposal issues, the concept of resilience in the implementation of BESS can expand beyond technical performance. This expansion would extend to multiobjective measurement and could eventually lead to a co-design framework for OWFs integrated with BESS [78].

This study helps bridge the gap between the analysis of the OWF topology and considerations to improve resilience. The optimal BESS capacity is no longer treated as a deterministic modeling outcome;

Table 7
Hourly load data in percentage of installed capacity of OWF (%) [67].

Time	Summer Wkdy	Summer Wknd	Monsoon Wkdy	Monsoon Wknd	Autumn Wkdy	Autumn Wknd	Winter Wkdy	Winter Wknd	Average
1:00 am	81	66	86	65	80	71	80	73	75.25
2:00 am	77	68	86	63	81	70	75	64	73.00
3:00 am	80	72	84	72	82	73	78	65	75.75
4:00 am	79	72	83	77	84	72	80	65	76.50
5:00 am	79	75	84	82	86	77	83	67	79.13
6:00 am	82	75	84	88	86	81	86	75	82.13
7:00 am	84	77	87	90	89	83	89	80	84.88
8:00 am	87	78	90	93	90	86	90	87	87.63
9:00 am	90	83	95	94	92	94	92	94	91.75
10:00 am	94	89	98	94	94	94	95	97	94.38
11:00 am	95	88	99	96	96	94	94	97	94.88
12:00 pm	94	88	98	97	95	94	96	98	95.00
1:00 pm	93	88	96	96	94	89	96	97	93.63
2:00 pm	91	86	92	94	92	86	94	89	90.50
3:00 pm	88	84	89	94	90	84	90	86	88.13
4:00 pm	87	86	87	88	90	86	90	81	86.88
5:00 pm	91	93	90	89	92	90	93	85	90.38
6:00 pm	95	97	95	94	100	96	96	96	96.13
7:00 pm	98	100	99	100	100	100	100	100	99.63
8:00 pm	100	95	100	96	100	98	100	100	98.63
9:00 pm	97	93	99	98	97	91	99	94	96.00
10:00 pm	94	85	97	95	93	85	94	92	91.88
11:00 pm	84	72	90	82	83	70	84	80	80.63
12:00 am	88	74	93	73	83	71	83	80	80.63

Table 8
Nomenclature for the minimal spanning tree model (Section 3.2).

Type	Symbol	Description	Unit
Set	Ω^{Clu}	Set of clusters under a fixed clustering level	–
Set	Clu_c	Set of WTs inside the cluster c	–
Parameter	$D(WT_i, WT_j)$	The (Euclidean) distance between the i th WT and the j th WT	km
Parameter	X_{WT_i}, Y_{WT_i}	X and Y coordinates of the i th WT	–
Parameter	$AM(i,j)$	The adjacent matrix of the entire OWF	binary
Parameter	$card(Clu_c)$	The number of nodes (WTs) inside the cluster c	–
Parameter	M_c	Required number of connecting acres inside cluster c	–
Parameter	$b_i^{Clu_c}$	Right-hand side (exogenous net inflow) of WT_i inside cluster c	–
Variable	$F_{j,i}^{Clu_c}$	Flow from WT_i to WT_j inside the cluster c	–
Variable	$Link(WT_i, WT_j)$	Connection status between the i th WT and the j th WT	binary
Variable (intermediate)	$Length_c$	Square of total length of transmission cables connecting all WTs inside the cluster c	km^2

instead, the relationship between network configuration planning and resilient operations is thoroughly explored. In addition to the potential future expansions on system resilience mentioned above, these contributions also have the potential for significant improvements to the proposed model in several areas, including the construction of multiterminal OWFs and the coordination of other onshore energy production technologies.

CRediT authorship contribution statement

Weijie Pan: Writing – review & editing, Writing – original draft, Visualization, Validation, Software, Resources, Methodology, Investigation, Formal analysis, Data curation, Conceptualization. **Ekundayo Shittu:** Writing – review & editing, Validation, Supervision, Methodology, Funding acquisition, Conceptualization.

Declaration of competing interest

The authors declare that they have no known competing financial interests or personal relationships that could have appeared to influence the work reported in this paper.

Acknowledgments

This research was supported by the U.S. National Science Foundation (NSF) under Award 1847077. The authors also wish to acknowledge the support of Professor Inês Lima Azevedo from the Department of Energy Science & Engineering at Stanford University, United States.

Appendix A. Complete data for hourly demand profile

See Table 7.

Table 9
Nomenclature for the optimal cluster planning model (Section 3.2).

Type	Symbol	Description	Unit
Set	Ω^{Clu}	Set of clusters under a fixed cluster number	–
Set	Clu_c	Set of WTs inside the cluster c	–
Parameter	$C^{Sub-Ocp}$	Unit cost for transmission cables connecting SUB and OCP	$/km
Parameter	$C^{Clu-Sub}$	Unit cost for transmission cables connecting the cluster and SUB	$/km
Parameter	X_{Ocp}, Y_{Ocp}	X and Y coordinates of OCP	–
Parameter	$X^{WT_i^c}$, $Y^{WT_i^c}$	X and Y coordinates of the WT_i that belongs to the $Cluster_c$	–
Variable	X_{Sub}, Y_{Sub}	X and Y coordinates of SUB	–
Variable	$Link(WT_i^c, Sub)$	Connection between WT_i^c and SUB	binary
Variable (intermediate)	$D(Sub, Ocp)$	The (Euclidean) distance between SUB and OCP	km
Variable (intermediate)	$D(WT_i^c, Sub)$	The (Euclidean) distance between the WT_i^c and SUB	km

Table 10
Nomenclature for scenario generation process (Section 3.3).

Type	Symbol	Description	Unit
Set	Ω^{Time}	Set of time	–
Set	Ω^{Scen}	Set of scenarios	–
Set	$\Omega^{WT_{f,s}}$	Set of impacted WTs under scenario s	–
Set	$\Omega^{T_{f,s}}$	Set of fault occurrence time under scenario s	–
Index	$Level_L$	The Lth level of power curtailment severity	–
Index	Com_i	The ith combination of time dimensions of stochastic process of HILP events	–
Parameter	Cap_{OWF}^{Ins}	Total installed capacity of the entire OWF	kW
Parameter	Cap_i^{Ins}	Installed capacity of WT_i	kW
Parameter	$Cap_{k,T}^{Ins}$	Installed capacity of the affected WT_k at the degraded system time T	kW
Variable	$Cap_{s,t}^{Gen}$	Real-time generation capacity of OWF in scenario s at time t	kW
Variable	Pr_s	Probability of scenario s	–

Table 11
Nomenclature for the optimal BESS capacity model (Section 3.4).

Type	Symbol	Description	Unit
Parameter	C^{Ins}	Levelized cost for utility-scale BESS	$/kWh
Parameter	C^{Rec}	Unit post-disaster recovery cost for the affected transmission line	$/km h
Parameter	C^{Rew}	Unit reward for storing battery energy	$/kWh
Parameter	De_t	Energy demand at time t	kWh
Parameter	$Cap_{s,t}^{Gen}$	Real-time generation capacity of OWF in scenario s at time t	kW
Parameter	T_s^{fd}	Duration of system degradation in scenario s	h
Parameter	$TL(Level_s)^f$	Total length of impacted transmission lines in scenario s	km
Parameter	∇_t	Modeling time step	h
Parameter	Pr_s	Probability of scenario s	–
Variable (first-stage)	$\overline{B}$	Capacity of battery	kWh
Variable (second-stage)	$B_{s,t}$	Energy stored in the battery in scenario s at time t	kWh
Variable (second-stage)	$B_{s,t}^{Discha}$	Energy discharged from the battery in scenario s at time t	kWh
Variable (second-stage)	$P_{s,t}^{Gen}$	Power generation from OWF in scenario s at time t	kW
Variable (second-stage)	$P_{s,t}^{Cha}$	Power generation for charging the battery in scenario s at time t	kW
Variable (second-stage)	$SOC_{s,t}$	State of charging in scenario s at time t	binary
Variable (second-stage)	$SOD_{s,t}$	State of discharging in scenario s at time t	binary

Appendix B. Nomenclature tables

See Tables 8–11.

Data availability

Data will be made available on request.

References

[1] Gholami M, Shahryari O, Rezaei N, Bevrani H. Optimum storage sizing in a hybrid wind-battery energy system considering power fluctuation characteristics. J Energy Storage 2022;52:104634. http://dx.doi.org/10.1016/j.est.2022.104634.

[2] Shittu E, Weigelt C. When the wind blows: Incumbents' sourcing strategies for wind power. IEEE Trans Eng Manage 2022;1–20. http://dx.doi.org/10.1109/TEM.2022.3159113.

[3] Shittu E, Weigelt C. Accessibility in sustainability transitions: U.S. electric utilities' deployment of solar. Energy Policy 2022;165:112942. http://dx.doi.org/10.1016/j.enpol.2022.112942.

[4] Shittu E, Baker E. Optimal energy R&D portfolio investments in response to a carbon tax. IEEE Trans Eng Manage 2010;57(4):547–59. http://dx.doi.org/10.1109/TEM.2009.2023107.

[5] Knight UG. Power systems in emergencies: From contingency planning to crisis management. Chichester, England ; New York: John Wiley; 2001.

[6] Bizon N, Mahdavi Tabatabaei N, Najafi Ravadanegh S, editors. Power systems resilience: Modeling, analysis and practice, In: Power systems, 1st ed.. Cham: Springer International Publishing : Imprint: Springer; 2019, http://dx.doi.org/10.1007/978-3-319-94442-5.

[7] Pan W, Shittu E. Policies and power systems resilience under time-based stochastic process of contingencies in networked microgrids. IEEE Trans Eng Manage 2023;1–21. http://dx.doi.org/10.1109/TEM.2023.3325188.

[8] Shittu E, Parker G, Jiang X. Energy technology investments in competitive and regulatory environments. Environ Syst Decis 2015;35(4):453–71. http://dx.doi.org/10.1007/s10669-015-9569-y.

[9] DeLuque I, Shittu E. Generation capacity expansion under demand, capacity factor and environmental policy uncertainties. Comput Ind Eng 2019;127:601–13. http://dx.doi.org/10.1016/j.cie.2018.10.051.

[10] Zuo T, Zhang Y, Xie X, Meng K, Tong Z, Dong ZY, Jia Y. A review of optimization technologies for large-scale wind farm planning with practical and prospective concerns. IEEE Trans Ind Inf 2023;19(7):7862–75. http://dx.doi.org/10.1109/TII.2022.3217282.

[11] Breeze P. Chapter 11 - Wind power. In: Breeze P, editor. Power generation technologies (third edition). Newnes; 2019, p. 251–73. http://dx.doi.org/10.1016/B978-0-08-102631-1.00011-0.

[12] Global Wind Energy Council. Global wind report 2023. 2023, URL https://gwec.net/globalwindreport2023/.

[13] Paul S, Nath AP, Rather ZH. A Multi-objective planning framework for co-ordinated generation from offshore wind farm and battery energy storage system. IEEE Trans Sustain Energy 2020;11(4):2087–97. http://dx.doi.org/10.1109/TSTE.2019.2950310.

[14] Department of Energy. Offshore wind market report: 2023 Edition. URL https://www.energy.gov/eere/wind/articles/offshore-wind-market-report-2023-edition.

[15] Shield SA, Quiring SM, Pino JV, Buckstaff K. Major impacts of weather events on the electrical power delivery system in the United States. Energy 2021;218:119434. http://dx.doi.org/10.1016/j.energy.2020.119434.

[16] Anderson F, Dawid R, McMillan D, Cava DG. On the sensitivity of wind turbine failure rate estimates to failure definitions. J Phys: Conf Ser 2023;2626(1):012025. http://dx.doi.org/10.1088/1742-6596/2626/1/012025.

[17] Warnock J, McMillan D, Pilgrim J, Shenton S. Failure rates of offshore wind transmission systems. Energies 2019;12(14):2682. http://dx.doi.org/10.3390/en12142682, Number: 14 Publisher: Multidisciplinary Digital Publishing Institute.

[18] Giussani R. Best practice guideline for the complete condition monitoring (CM) of Offshore Wind Farm (OWF) cable networks. 2015.

[19] Arikan Y, Campbell M. Maximising power cable reliability for offshore wind. 2022, URL https://acteon.com/blog/maximising-power-cable-reliability-for-offshore-wind/.

[20] Maples B, Saur G, Hand M, van de Pieterman R, Obdam T. Installation, operation, and maintenance strategies to reduce the cost of offshore wind energy. Tech. rep., 2013, URL https://www.osti.gov/biblio/1087778/.

[21] Besnard F, Fischer K, Tjernberg LB. A model for the optimization of the maintenance support organization for offshore wind farms. IEEE Trans Sustain Energy 2013;4(2):443–50. http://dx.doi.org/10.1109/TSTE.2012.2225454.

[22] Perera ATD, Nik VM, Chen D, Scartezzini J-L, Hong T. Quantifying the impacts of climate change and extreme climate events on energy systems. Nat Energy 2020;5(2):150–9. http://dx.doi.org/10.1038/s41560-020-0558-0.

[23] Panteli M, Mancarella P. The grid: stronger, bigger, smarter?: presenting a conceptual framework of power system resilience. IEEE Power Energy Mag 2015;13(3):58–66. http://dx.doi.org/10.1109/MPE.2015.2397334.

[24] Jufri FH, Widiputra V, Jung J. State-of-the-art review on power grid resilience to extreme weather events: Definitions, frameworks, quantitative assessment methodologies, and enhancement strategies. Appl Energy 2019;239:1049–65. http://dx.doi.org/10.1016/j.apenergy.2019.02.017.

[25] Feng W, Tuan LA, Tjernberg LB, Mannikoff A, Bergman A. A new approach for benefit evaluation of multiterminal VSC–HVDC using a proposed mixed AC/DC optimal power flow. IEEE Trans Power Deliv 2014;29(1):432–43. http://dx.doi.org/10.1109/TPWRD.2013.2267056.

[26] MacIver C, Bell KRW, Nedić DP. A reliability evaluation of offshore HVDC grid configuration options. IEEE Trans Power Deliv 2016;31(2):810–9. http://dx.doi.org/10.1109/TPWRD.2015.2437717.

[27] Quinonez-Varela G, Ault GW, Anaya-Lara O, McDonald JR. Electrical collector system options for large offshore wind farms. IET Renew Power Gener 2007;1(2):107–14.

[28] Shittu E, Tibrewala A, Kalla S, Wang X. Meta-analysis of the strategies for self-healing and resilience in power systems. Adv Appl Energy 2021;4:100036. http://dx.doi.org/10.1016/j.adapen.2021.100036.

[29] Hussain A, Bui V-H, Kim H-M. Microgrids as a resilience resource and strategies used by microgrids for enhancing resilience. Appl Energy 2019;240:56–72. http://dx.doi.org/10.1016/j.apenergy.2019.02.055.

[30] Li Z, Shahidehpour M, Aminifar F, Alabdulwahab A, Al-Turki Y. Networked microgrids for enhancing the power system resilience. Proc IEEE 2017;105(7):1289–310. http://dx.doi.org/10.1109/JPROC.2017.2685558.

[31] Teleke S, Baran ME, Huang A, Bhattacharya S, Anderson L. Control strategies for battery energy storage for wind farm dispatching. IEEE Trans Energy Convers 2009;24(3):725–32. http://dx.doi.org/10.1109/TEC.2009.2016000.

[32] Hauer I, Balischewski S, Ziegler C. Design and operation strategy for multi-use application of battery energy storage in wind farms. J Energy Storage 2020;31:101572. http://dx.doi.org/10.1016/j.est.2020.101572.

[33] Pagnani D, Kocewiak L, Hjerrild J, Blaabjerg F, Bak CL, Blasco-Gimenez R, Martínez-Turégano J. Wind turbine and battery storage interoperability to provide black start by offshore wind. CIGRE Sci Eng 2023;29:1–26.

[34] Pagnani D, Kocewiak L, Hjerrild J, Blaabjerg F, Bak CL. Integrating black start capabilities into offshore wind farms by grid-forming batteries. IET Renew Power Gener 2023;17(14):3523–35. http://dx.doi.org/10.1049/rpg2.12667.

[35] Naemi M, Davis D, Brear MJ. Optimisation and analysis of battery storage integrated into a wind power plant participating in a wholesale electricity market with energy and ancillary services. J Clean Prod 2022;373:133909. http://dx.doi.org/10.1016/j.jclepro.2022.133909.

[36] Liu M, Qin J, Lu D-G, Zhang W-H, Zhu J-S, Faber MH. Towards resilience of offshore wind farms: A framework and application to asset integrity management. Appl Energy 2022;322:119429. http://dx.doi.org/10.1016/j.apenergy.2022.119429.

[37] Shakoor R, Hassan MY, Raheem A, Wu Y-K. Wake effect modeling: A review of wind farm layout optimization using Jensen's model. Renew Sustain Energy Rev 2016;58:1048–59. http://dx.doi.org/10.1016/j.rser.2015.12.229.

[38] Pérez-Rúa J-A, Cutululis NA. Electrical cable optimization in offshore wind farms—A review. IEEE Access 2019;7:85796–811. http://dx.doi.org/10.1109/ACCESS.2019.2925873.

[39] Hou P, Zhu J, Ma K, Yang G, Hu W, Chen Z. A review of offshore wind farm layout optimization and electrical system design methods. J Mod Power Syst Clean Energy 2019;7(5):975–86. http://dx.doi.org/10.1007/s40565-019-0550-5.

[40] Pillai A, Chick J, Johanning L, Khorasanchi M, de Laleu V. Offshore wind farm electrical cable layout optimization. Eng Optim 2015;47(12):1689–708. http://dx.doi.org/10.1080/0305215X.2014.992892.

[41] Ziyaei P, Khorasanchi M, Sayyaadi H, Sadollah A. Minimizing the levelized cost of energy in an offshore wind farm with non-homogeneous turbines through layout optimization. Ocean Eng 2022;249:110859. http://dx.doi.org/10.1016/j.oceaneng.2022.110859.

[42] Paul S, Rather ZH. A novel approach for optimal cabling and determination of suitable topology of MTDC connected offshore wind farm cluster. Electr Power Syst Res 2022;208:107877. http://dx.doi.org/10.1016/j.epsr.2022.107877.

[43] Dahmani O, Bourguet S, Machmoum M, Guérin P, Rhein P, Jossé L. Optimization of the connection topology of an offshore wind farm network. IEEE Syst J 2015;9(4):1519–28. http://dx.doi.org/10.1109/JSYST.2014.2330064.

[44] Li J, Song Z, Wang X, Wang Y, Jia Y. A novel offshore wind farm typhoon wind speed prediction model based on PSO–Bi-LSTM improved by VMD. Energy 2022;251:123848. http://dx.doi.org/10.1016/j.energy.2022.123848.

[45] Lu H, Ma X, Huang K, Azimi M. Prediction of offshore wind farm power using a novel two-stage model combining kernel-based nonlinear extension of the Arps decline model with a multi-objective grey wolf optimizer. Renew Sustain Energy Rev 2020;127:109856. http://dx.doi.org/10.1016/j.rser.2020.109856.

[46] Shin J-S, Kim J-O. Optimal design for offshore wind farm considering inner grid layout and offshore substation location. IEEE Trans Power Syst 2017;32(3):2041–8. http://dx.doi.org/10.1109/TPWRS.2016.2593501.

[47] Zuo T, Zhang Y, Meng K, Tong Z, Dong ZY, Fu Y. A two-layer hybrid optimization approach for large-scale offshore wind farm collector system planning. IEEE Trans Ind Inf 2021;17(11):7433–44. http://dx.doi.org/10.1109/TII.2021.3056428.

[48] Gong X, Kuenzel S, Pal BC. Optimal wind farm cabling. IEEE Trans Sustain Energy 2018;9(3):1126–36. http://dx.doi.org/10.1109/TSTE.2017.2771147.

[49] Chao H, Li T, Wang Y, Su Y, Liu F, Liang Z. Reliability evaluation for offshore wind farms considering seasonal characteristics and collection system failure. In: 2023 Panda forum on power and energy. PandaFPE, 2023, p. 80–4. http://dx.doi.org/10.1109/PandaFPE57779.2023.10141018.

[50] Feng Q, Zhao X, Fan D, Cai B, Liu Y, Ren Y. Resilience design method based on meta-structure: A case study of offshore wind farm. Reliab Eng Syst Saf 2019;186:232–44. http://dx.doi.org/10.1016/j.ress.2019.02.024.

[51] Rong J, Zhou M, Li G. Resilience-oriented restoration strategy by offshore wind power considering risk. CSEE J Power Energy Syst 2023;1–12. http://dx.doi.org/10.17775/CSEEJPES.2022.07710.

[52] Liang Y, Lin S, Feng X, Liu M, Su L, Zhang B. Optimal resilience enhancement dispatch of a power system with multiple offshore wind farms considering uncertain typhoon parameters. Int J Electr Power Energy Syst 2023;153:109337. http://dx.doi.org/10.1016/j.ijepes.2023.109337.

[53] Haddadi M, Rabiee A, Nikkhah S. Location-based uncertainty management of offshore wind farms: A multiple radius robust decision making. Int J Electr Power Energy Syst 2022;136:107667. http://dx.doi.org/10.1016/j.ijepes.2021.107667.

[54] Baker K, Hug G, Li X. Energy storage sizing taking Into account forecast uncertainties and receding horizon operation. IEEE Trans Sustain Energy 2017;8(1):331–40. http://dx.doi.org/10.1109/TSTE.2016.2599074.

[55] Wan C, Qian W, Zhao C, Song Y, Yang G. Probabilistic forecasting based sizing and control of hybrid energy storage for wind power smoothing. IEEE Trans Sustain Energy 2021;12(4):1841–52. http://dx.doi.org/10.1109/TSTE.2021.3068043.

[56] Hou P, Hu W, Soltani M, Chen Z. Optimized placement of wind turbines in large-scale offshore wind farm using Particle Swarm Optimization algorithm. IEEE Trans Sustain Energy 2015;6(4):1272–82. http://dx.doi.org/10.1109/TSTE.2015.2429912.

[57] Jafari M, Botterud A, Sakti A. Estimating revenues from offshore wind-storage systems: The importance of advanced battery models. Appl Energy 2020;276:115417. http://dx.doi.org/10.1016/j.apenergy.2020.115417.

[58] RENOLIT Group. Wind turbines maintenance and reparation. URL https://www.renolit.com/en/industries/wind-energy/renolit-cp/wind-turbines-maintenance-and-reparation/wind-turbines-maintenance-and-reparation.

[59] Jain AK, Dubes RC. Algorithms for clustering data. USA: Prentice-Hall, Inc.; 1988.
[60] Mohammadi F, Sahraei-Ardakani M. Multidimensional scenario selection for power systems with stochastic failures. IEEE Trans Power Syst 2020;35(6):4528–38. http://dx.doi.org/10.1109/TPWRS.2020.2990877.
[61] Ghasemi M, Kazemi A, Gilani MA, Shafie-Khah M. A stochastic planning model for improving resilience of distribution system considering master-slave distributed generators and network reconfiguration. IEEE Access 2021;9:78859–72. http://dx.doi.org/10.1109/ACCESS.2021.3083698.
[62] Pop PC. The generalized minimum spanning tree problem: An overview of formulations, solution procedures and latest advances. European J Oper Res 2020;283(1):1–15. http://dx.doi.org/10.1016/j.ejor.2019.05.017.
[63] Kalvelagen E. Yet another math programming consultant: Minimum spanning trees in math programming models. 2021, URL https://yetanothermathprogrammingconsultant.blogspot.com/2021/03/minimum-spanning-trees-in-math.html.
[64] Li H, Ren Z, Fan M, Li W, Xu Y, Jiang Y, Xia W. A review of scenario analysis methods in planning and operation of modern power systems: Methodologies, applications, and challenges. Electr Power Syst Res 2022;205:107722. http://dx.doi.org/10.1016/j.epsr.2021.107722.
[65] Parc éolien en mer de Saint-Nazaire | Découvrir le projet éolien de Saint-Nazaire. 2023, URL https://parc-eolien-en-mer-de-saint-nazaire.fr/.
[66] FINO3. Research platform in the North Sea and the baltic no. 3. URL https://www.fino3.de/en/.
[67] Alam MN, Chakrabarti S, Liang X. A benchmark test system for networked microgrids. IEEE Trans Ind Inf 2020;16(10):6217–30. http://dx.doi.org/10.1109/TII.2020.2976893.
[68] Meng Y, Yan S, Wu K, Ning L, Li X, Wang X, Wang X. Comparative economic analysis of low frequency AC transmission system for the integration of large offshore wind farms. Renew Energy 2021;179:1955–68. http://dx.doi.org/10.1016/j.renene.2021.07.137.
[69] Colthorpe A. Behind the numbers: the rapidly falling LCOE of battery storage. 2020, URL https://www.energy-storage.news/behind-the-numbers-the-rapidly-falling-lcoe-of-battery-storage/.
[70] BloombergNEF. Battery power's latest plunge in costs threatens coal, gas. 2019, URL https://about.bnef.com/blog/battery-powers-latest-plunge-costs-threatens-coal-gas/.
[71] US Energy Information Administration. Electric power monthly. 2023, URL https://www.eia.gov/electricity/monthly/index.php.
[72] US Energy Information Administration. Electricity generation, capacity, and sales in the United States. 2023, URL https://www.eia.gov/energyexplained/electricity/electricity-in-the-us-generation-capacity-and-sales.php.
[73] MathWorks. Agglomerative hierarchical cluster tree - MATLAB linkage. URL https://www.mathworks.com/help/stats/linkage.html.
[74] International Energy Agency. Offshore wind outlook 2019. Tech. rep., 2019, URL https://www.iea.org/reports/offshore-wind-outlook-2019.
[75] Determining the optimal number of clusters: 3 must know methods. URL https://www.datanovia.com/en/lessons/determining-the-optimal-number-of-clusters-3-must-know-methods/.
[76] Umunnakwe A, Huang H, Oikonomou K, Davis KR. Quantitative analysis of power systems resilience: Standardization, categorizations, and challenges. Renew Sustain Energy Rev 2021;149:111252. http://dx.doi.org/10.1016/j.rser.2021.111252.
[77] Tao S, Zhang C, Feijóo-Lorenzo AE, Kim V. Optimal design and operation of a wind farm/battery energy storage considering demand side management. IET Renew Power Gener 2024;1–11. http://dx.doi.org/10.1049/rpg2.12951.
[78] Aziz MJ, Gayme DF, Johnson K, Knox-Hayes J, Li P, Loth E, Pao LY, Sadoway DR, Smith J, Smith S. A co-design framework for wind energy integrated with storage. Joule 2022;6(9):1995–2015. http://dx.doi.org/10.1016/j.joule.2022.08.014.